The Astrophysical Journal, 653:1226–1240, 2006 December 20

THE ELECTRON TEMPERATURE GRADIENT IN THE GALACTIC DISK

Cintia Quireza,[1,2,3] Robert T. Rood,[3] T. M. Bania,[4] Dana S. Balser,[5] and Walter J. Maciel[2]

Received 2006 July 21; accepted 2006 August 31

ABSTRACT

We derive the electron temperature gradient in the Galactic disk, using a sample of H II regions that spans Galactocentric distances of 0–17 kpc. The electron temperature was calculated using high-precision radio recombination line and continuum observations for more than 100 H II regions. Nebular Galactocentric distances were calculated in a consistent manner, using the radial velocities measured by our radio recombination line survey. The large number of nebulae widely distributed over the Galactic disk, together with the uniformity of our data, provide a secure estimate of the present electron temperature gradient in the Milky Way. Because metals are the main coolants in the photoionized gas, the electron temperature along the Galactic disk should be directly related to the distribution of heavy elements in the Milky Way. Our best estimate of the electron temperature gradient is derived from a sample of 76 sources for which we have the highest quality data. The present gradient in electron temperature has a minimum at the Galactic center and rises at a rate of 287 ± 46 K kpc^{-1}. There are no significant variations in the value of the gradient as a function of Galactocentric radius or azimuth. The scatter we find in the H II region electron temperatures at a given Galactocentric radius is not due to observational error, but rather to intrinsic fluctuations in these temperatures, which are almost certainly due to fluctuations in the nebular heavy-element abundances. Comparing the H II region gradient with the much steeper gradient found for planetary nebulae suggests that the electron temperature gradient evolves with time, becoming flatter as a consequence of the chemical evolution of the Milky Way's disk.

Subject headings: H II regions — ISM: abundances — ISM: clouds — ISM: evolution — ISM: lines and bands — ISM: structure — nuclear reactions, nucleosynthesis, abundances — radio lines: ISM

1. INTRODUCTION

Churchwell & Walmsley (1975) pioneered H II region radio recombination line (RRL) studies of the relationship between nebular electron temperatures, T_e, and Galactocentric distance, $R_{\rm Gal}$ (e.g., Churchwell et al. 1978; Wink et al. 1983; Shaver et al. 1983). Because RRLs are not obscured by interstellar dust, relatively faint H II regions at extremely large distances from the Sun could be detected. They found that there was a Galactic temperature gradient wherein T_e is low in the Galactic center and increases with $R_{\rm Gal}$. Such a gradient was first observed in other nearby spiral galaxies by Searle (1971), Rubin et al. (1972), and Smith (1975). This Milky Way electron temperature gradient was confirmed by radio continuum emission (Omar et al. 2002) and by [O III] forbidden line optical observations (Peimbert et al. 1978; Deharveng et al. 2000). Because heavy elements cool photoionized gas, H II region electron temperatures are directly related to the heavy-element abundance: low T_e corresponds to higher heavy-element abundances because of the greater cooling rate and vice versa. Consequently, T_e gradients should be inversely related to metal abundance gradients (but see § 6). Because there has been more stellar processing in the inner Galaxy, one expects that on average the metallicity decreases as a function of $R_{\rm Gal}$.

The existence of a Galactic gradient in H II region electron temperature is now firmly established. Nevertheless, there are still uncertainties in the magnitude of the gradient and the possible existence of real variations, both in $R_{\rm Gal}$ and in Galactic azimuth, of nebular T_e. Extant RRL studies yield T_e gradients that, roughly, vary from 250 to 440 K kpc^{-1}. Discrepancies in the results obtained from different studies may be attributed to several factors, including the source sample and the T_e derivation. Since the exact value of the T_e gradient provides an important constraint on models for Galactic chemical evolution, it must be determined as accurately as possible.

Here we derive H II region electron temperatures based on RRL and continuum data for a large sample of nebulae widely distributed across the Galactic disk. The RRL data are of unprecedented sensitivity compared with previous studies. We examine anew the Galactic temperature gradient and assess the magnitude and origin of the T_e dispersion at a given $R_{\rm Gal}$. In § 2 we describe our H II region sample. In § 3 we derive the nebular electron temperatures and discuss non-LTE effects. Nebular Galactocentric distances, $R_{\rm Gal}$, and heliocentric distances, $d_{\rm Sun}$, are derived in § 4. In § 5 our new determination of the electron temperature gradient in the Galactic disk is made. Here we also investigate a possible spatial variation of this gradient. We discuss the astrophysical implications of our efforts in § 6.

2. OBSERVATIONAL SAMPLE

Our H II region sample data are described by Quireza et al. (2006 and references therein). The RRL and continuum data result from two different experiments. Neither was targeted to investigate radial gradients in the Galactic disk. The first one (hereafter referred to as the ^{3}He survey) is a study of the abundance of ^{3}He in the Milky Way interstellar medium (Rood et al. 1984; Bania et al. 1987, 1997; Balser et al. 1994) using the hyperfine transition of $^3He^+$ at 8.665 GHz. The observing techniques required that a number of RRLs be measured simultaneously with the $^3He^+$ transition. These RRLs were used both to monitor the system performance and to measure the spectral baseline frequency structure. As a consequence of the large integration times (over

[1] Observatório Nacional, Rua General José Cristino 77, 20921-400 Rio de Janeiro, RJ, Brazil; quireza@on.br.
[2] Instituto de Astronomia, Geofísica e Ciências Atmosféricas (IAG), Universidade de São Paulo, Rua do Matão 1226, 05508-900 São Paulo, SP, Brazil.
[3] Astronomy Department, University of Virginia, P.O. Box 3818, Charlottesville, VA 22903-0818.
[4] Department of Astronomy, Institute for Astrophysical Research, Boston University, 725 Commonwealth Avenue, Boston, MA 02215.
[5] National Radio Astronomy Observatory, P.O. Box 2, Green Bank, WV 24944.

100 hr in many cases) accumulated during this experiment, we obtained extremely high sensitivity measurements of the He91α and H91α ($\Delta n = 1$) RRL transitions for a significant number of Galactic H II regions. The second experiment (hereafter referred to as the C II survey) is a study of C II recombination lines in photodissociation (PDR) regions surrounding the H II regions. For this survey, we simultaneously observed the H, He, and C 91α and 92α RRL transitions. Since recombination lines of the same order with similar principal quantum numbers, such as H91α and H92α or He91α and He92α, should have the same intensity, we averaged the 91α and 92α spectra to attain higher sensitivity (see Quireza et al. [2006] for details).

All observations were made near 8.6 GHz (3.5 cm) with the National Radio Astronomy Observatory (NRAO)[6] 140 ft (43 m) telescope in Green Bank, WV, which has a half-power beam width (HPBW) of 3.′20 at this frequency. Our sample has 106 sources: 47 nebulae from the ^{3}He survey and 66 from the C II survey. (There are seven objects in common.)

The quantities needed to derive nebular electron temperatures are the H91α line peak intensities, T_L, the line full width at half-maximum, Δv, and the continuum intensity, T_C. These parameters and their errors may be found in Quireza et al. (2006). There we also assess the quality of our data: we have defined quality factors (QFs) for both spectral line and continuum data. Because we cannot quantify the systematic errors, these QFs provide a qualitative measure of them. By choosing subsets of data with different QFs, we can assess the importance of systematic errors on our conclusions reported here. Quality factor *A* sources refer to our best data: the spectra are almost noiseless, and systematic errors appear to be negligible. The QF decreases from *A* to *E*. We judge QFs *D* and *E* to be of too low confidence to be included in our analysis here.

3. DETERMINATION OF THE PHYSICAL PARAMETERS

3.1. *LTE Electron Temperature*

The electron temperature of each nebula is derived from the observed RRL-to-continuum ratio, T_L/T_C. We model our sources as homogeneous, isothermal spheres. This approximation allows us to calculate the electron temperature without having to know the distance to the source. If the distance is known, many other nebular physical properties, such as electron density and emission measure, can be derived.

Most of the emission observed from H II regions is continuum radiation produced by free-free thermal bremsstrahlung in the plasma. At high frequencies, the nebular gas is optically thin, and the ratio between the brightness temperature of a recombination line and that of the free-free emission continuum depends on the radio frequency and the gas temperature, but is independent of the electron density, n_e. Thus, the observed T_L/T_C may be used to estimate the electron temperature of the H II region (Goldberg 1968; Rohlfs & Wilson 2000). Assuming local thermodynamic equilibrium (LTE) and negligible pressure broadening of the lines by electron impacts, the electron temperature is given by

$$\left(\frac{T_e^*}{\mathrm{K}}\right) = \left\{ 7103.3 \left(\frac{\nu_L}{\mathrm{GHz}}\right)^{1.1} \left[\frac{T_C}{T_L(\mathrm{H}^+)}\right] \left[\frac{\Delta v(\mathrm{H}^+)}{\mathrm{km\ s^{-1}}}\right]^{-1} \times \left[1 + \frac{n(^4\mathrm{He}^+)}{n(\mathrm{H}^+)}\right]^{-1} \right\}^{0.87}, \quad (1)$$

where we distinguish the LTE temperature, T_e^*, from the electron temperature corrected for non-LTE and high-density effects, T_e. The line frequency, $\nu_L = 8.584823$ GHz, corresponds to the rest frequency of the H91α recombination line. Here T_C (K) is the continuum antenna temperature; T_L (K) and Δv (km s^{-1}) are the H91α recombination line antenna temperature and FWHM line width, respectively. The $n(^4\mathrm{He}^+)/n(\mathrm{H}^+)$ ionic abundance ratio was calculated using the areas of Gaussian fits to the H and He recombination lines (Peimbert et al. 1992):

$$\frac{n(^4\mathrm{He}^+)}{n(\mathrm{H}^+)} = \frac{T_L(^4\mathrm{He}^+)\Delta v(^4\mathrm{He}^+)}{T_L(\mathrm{H}^+)\Delta v(\mathrm{H}^+)}. \quad (2)$$

For a small number of objects, we do not have good measurements of the ^{4}He transition. In these cases, we used a constant value of 0.07 ± 0.02 for the $n(^4\mathrm{He}^+)/n(\mathrm{H}^+)$ abundance ratio. This ratio is the average of our 80 best QF (*A*, *B*, and *C*) sources and is typical for H II regions (Churchwell et al. 1974; Shaver et al. 1983).

The nebular LTE electron temperatures and their errors, σ_{T_e}—together with the Galactocentric distances R_{Gal}, heliocentric distances d_{Sun}, and the $n(^4\mathrm{He}^+)/n(\mathrm{H}^+)$ ionic abundance ratios—are listed in Table 1. Also given are the name of the source and some of its physical properties, including the spherical angular size Θ_{diam}, linear diameter *D*, flux density S_ν, continuum brightness temperature T_C^B, and electron density n_e (see the discussion below). Each nebula's survey membership (either ^{3}He or C II) is indicated.

The electron temperature errors were derived by propagating the Gaussian fitting errors for the line and continuum measurements. These σ_{T_e} errors vary from 0.3% to 17.8% (2.2% on average). For our best QF data, σ_{T_e} errors vary from 0.4% to 11.0% (1.3% on average). These are lower limits to the temperature errors. Due to baseline problems and complex nebular structures, uncertainties in continuum measurements are certainly larger than the one we estimate, reaching 10% or even 20% in the worst cases. Since we have no way to quantify systematic uncertainties, we use the quality factors to estimate the effect of the systematic errors on the electron temperatures. The QFs for continuum and spectral-line parameters are listed, in this order, in Table 1.

The continuum observing mode can also affect the uncertainty in the measurements. We made continuum measurements using both the switched power (SP) and total power (TP) techniques. In Quireza et al. 2006, we point out that as a source was tracked across the sky, we interleaved the recombination line and SP continuum measurements such that both the continuum and line data span the same hour angle ranges and experience the same weather conditions. Thus, the line and continuum data would need identical corrections for telescope gain and atmospheric opacity. When calculating source properties that depend on the line-to-continuum ratio, such as the electron temperature, Quireza et al. (2006) suggested using SP continuum measurements. We therefore normally use SP continuum observations to calculate T_e^*, because many telescope effects are canceled in the line-to-continuum ratio. We did not have SP continuum measurements for a small number of our sources and had to use TP continuum data to calculate T_e^*. We estimate that the use of TP continuum data should give at most a $\sim$20% uncertainty in T_e^*. The observing mode used is listed in Table 1 for each nebula.

Accurate calculations of T_e should incorporate non-LTE effects, including departures from LTE, stimulated emission, and pressure broadening from electron impacts. These corrections for non-LTE effects are sensitive to the local density and thus the H II region geometry. Nevertheless, it has been shown that under

[6] The National Radio Astronomy Observatory is a facility of the National Science Foundation, operated under cooperative agreement by Associated Universities, Inc.

TABLE 1

PHYSICAL PROPERTIES OF GALACTIC H II REGIONS

Source	Name	R_{Gal} (kpc)	d_{Sun} (kpc)	Θ_{diam} (arcmin)	D (pc)	$n(^4He^+)/n(H^+)$	S_ν (Jy)	T_C^B (K)	n_e (cm^{-3})	T_e^{*a} (K)	Mode[b]	QFs[c]	Survey
G0.605+0.325.....	...	11.5	20.0	5.7	33.2	0.065 ± 0.025	0.8	0.2	13.2	6600 ± 320	TP	B, E	^{3}He
G0.665−0.035.....	Sgr B2	0.4	8.9	4.8	12.3	0.038 ± 0.014	40.3	17.3	194.7	8170 ± 180	SP	A, C	^{3}He
G1.13−0.1.....	...	0.1	8.5	7.6	18.7	0.065 ± 0.008	10.6	1.8	50.0	7130 ± 70	SP	C, B	^{3}He
G2.90+0.0.....	...	10.7	19.2	7.9	44.2	0.052 ± 0.014	1.3	0.2	10.1	4840 ± 140	TP	C, D	^{3}He
G3.270−0.101.....	...	5.5	14.0	7.4	30.0	0.077 ± 0.011	4.0	0.7	24.9	7440 ± 280	TP	B, C	^{3}He
G5.899−0.427.....	...	6.1	14.5	5.9	25.0	0.079 ± 0.010	18.8	5.2	78.9	11,130 ± 170	SP	B, C	C II
G5.956−1.265.....	...	7.8	16.2	11.6	54.8	0.074 ± 0.003	35.1	2.5	30.9	3420 ± 30	TP	C, B	C II
G5.973−1.178.....	M8	7.8	16.2	5.6	26.3	0.073 ± 0.005	32.9	10.3	103.1	8180 ± 70	SP	B, B	C II
G8.137+0.228.....	...	5.2	3.4	2.7	2.7	0.088 ± 0.006	5.8	7.9	276.7	7090 ± 60	SP	A, C	C II
G10.159−0.34.....	W31 A	6.6	14.7	4.6	19.6	0.034 ± 0.002	44.7	20.8	164.4	6830 ± 30	SP	A, A	C II
G10.315−0.15.....	...	7.0	15.2	4.1	18.2	0.070 ± 0.005	12.0	6.9	98.6	6800 ± 40	SP	A, B	C II
G10.617−0.38.....	W31 B	8.9	17.1	4.6	22.7	0.059 ± 0.004	9.9	4.6	76.3	9810 ± 90	SP	B, D	C II
G12.807−0.20.....	W33	5.0	12.9	2.8	10.6	0.047 ± 0.002	31.0	37.7	305.9	7620 ± 100	SP	A, C	C II
G13.875+0.28.....	...	4.3	4.5	2.1	2.7	0.059 ± 0.008	3.5	8.1	277.1	6960 ± 80	SP	A, C	C II
G14.626+0.08.....	...	5.1	12.9	12.6	47.0	0.061 ± 0.005	16.7	1.0	22.9	5510 ± 70	SP	C, D	C II
G15.035−0.68[d].....	M17 S	6.8	14.7	6.9	29.3	0.091 ± 0.011	272.2	56.4	215.4	5720 ± 60	TP	C, C	^{3}He
G15.095−0.71[d].....	M17 N	6.5	14.4	10.7	44.8	0.094 ± 0.004	450.3	38.3	154.9	9280 ± 120	SP	C, B	^{3}He
G15.181−0.62.....	...	6.8	14.6	8.3	35.3	0.059 ± 0.004	34.6	4.9	66.0	12,900 ± 160	TP	C, D	C II
G15.198−0.76.....	...	6.2	14.0	9.9	40.2	0.086 ± 0.006	20.6	2.1	38.3	9770 ± 120	TP	C, D	C II
G16.936+0.76[e].....	M16	6.2	2.4	10.7	7.5	0.105 ± 0.008	29.3	2.5	94.1	7880 ± 140	TP	C, D	C II
G16.936+0.76[d,e].....	M16	6.2	2.4	10.9	7.7	0.071 ± 0.008	30.5	2.5	92.6	7740 ± 120	TP	C, C	^{3}He
G16.984+0.93[d,e].....	M16 N	6.3	2.4	10.9	7.5	0.101 ± 0.009	25.3	2.1	83.8	6890 ± 60	TP	C, C	^{3}He
G16.995+0.86.....	...	6.3	2.3	12.8	8.7	0.067 ± 0.007	34.4	2.1	78.1	6970 ± 70	TP	C, C	C II
G18.143−0.28.....	...	4.7	4.1	4.1	4.9	0.047 ± 0.005	6.6	3.8	141.7	7180 ± 70	SP	B, C	C II
G18.686+1.96.....	S54	6.3	13.7	5.0	20.0	0.075 ± 0.006	8.4	3.3	65.2	7210 ± 60	SP	B, C	C II
G19.066−0.28.....	...	4.4	11.5	5.7	19.1	0.019 ± 0.004	7.2	2.1	51.4	5440 ± 70	SP	B, C	C II
G19.608−0.23.....	...	5.5	12.7	3.3	12.2	0.070 ± 0.005	6.5	5.8	109.4	6480 ± 80	SP	B, D	C II
G20.733−0.09.....	...	4.9	11.9	6.7	23.1	0.052 ± 0.005	8.5	1.9	43.9	5590 ± 90	SP	A, A	^{3}He
G23.421−0.21[e].....	...	3.7	6.3	5.6	10.2	0.130 ± 0.011	9.6	3.0	85.6	6630 ± 60	SP	B, C	C II
	...	3.7	6.3	5.6	10.2	0.049 ± 0.007	9.2	2.9	84.0	6370 ± 50	TP	B, B	^{3}He
G23.706+0.17.....	...	3.7	6.4	4.5	8.4	0.066 ± 0.009	3.0	1.5	66.7	6840 ± 110	TP	C, C	^{3}He
G24.467+0.48.....	...	3.9	6.1	2.6	4.6	0.070 ± 0.002	4.3	6.3	185.7	6370 ± 80	SP	A, B	C II
G24.484+0.21.....	...	3.5	7.7	10.5	23.5	0.062 ± 0.008	10.4	0.9	31.4	6360 ± 90	TP	C, D	^{3}He
G24.805+0.09.....	...	3.7	6.8	6.0	11.7	0.061 ± 0.009	7.5	2.1	65.2	5860 ± 90	SP	B, C	C II
G25.382−0.18[e].....	3C 385	5.2	11.4	5.2	17.3	0.059 ± 0.008	17.6	6.4	101.8	9280 ± 90	SP	A, D	C II
	3C 385	5.2	11.5	5.1	17.1	0.067 ± 0.004	16.9	6.3	98.5	7460 ± 70	SP	A, A	^{3}He
G25.766+0.21.....	...	3.7	7.3	7.6	16.1	0.029 ± 0.014	8.0	1.4	45.7	6120 ± 100	TP	C, C	^{3}He
G28.790+3.48.....	S64/W40	8.5	14.9	8.5	36.9	0.049 ± 0.005	26.2	3.5	51.0	8450 ± 70	SP	B, B	C II
G29.944−0.04.....	...	4.5	6.0	6.6	11.5	0.064 ± 0.006	17.7	4.0	92.8	6510 ± 90	SP	A, A	^{3}He
G30.776−0.03.....	W43	4.6	5.7	6.2	10.3	0.081 ± 0.003	59.5	15.0	193.3	7030 ± 50	SP	B, A	^{3}He
G32.797+0.19.....	...	7.7	13.3	2.6	9.9	0.099 ± 0.007	4.6	6.9	138.4	8930 ± 110	SP	A, D	C II
G34.254+0.14.....	NRAO 584	6.1	10.8	3.1	9.9	0.092 ± 0.006	14.0	13.9	197.8	8960 ± 60	SP	A, B	C II
G35.194−1.75.....	W48	6.4	2.8	1.9	1.6	0.078 ± 0.003	13.1	35.0	790.9	9100 ± 50	SP	A, A	C II
G40.505+2.54.....	S76	7.5	1.3	4.2	1.6	0.026 ± 0.005	4.2	2.4	195.6	7820 ± 100	SP	A, C	^{3}He
G43.169+0.00[e].....	W49	8.1	11.9	3.4	11.7	0.078 ± 0.003	43.9	37.5	294.3	8170 ± 40	SP	A, A	C II
	W49	8.1	11.9	3.7	12.7	0.087 ± 0.006	44.0	31.6	260.0	8410 ± 50	SP	C, A	^{3}He
G45.451+0.06.....	K47	6.5	8.3	3.2	7.7	0.079 ± 0.008	8.0	7.7	164.9	8550 ± 70	SP	A, C	C II
G46.495−0.25.....	...	6.5	7.8	6.7	15.1	0.091 ± 0.013	4.6	1.0	39.2	4860 ± 80	SP	A, C	^{3}He
G48.930−0.28.....	...	6.4	5.6	6.2	10.0	0.073 ± 0.006	20.1	5.1	118.2	8440 ± 60	SP	B, B	C II
G48.997−0.29.....	...	6.4	5.6	8.6	13.9	0.069 ± 0.003	26.4	3.5	82.4	8170 ± 50	SP	C, B	C II
G49.204−0.34.....	...	6.4	5.6	4.8	7.7	0.078 ± 0.004	18.4	8.0	169.9	9070 ± 70	SP	B, B	C II
G49.384−0.30[e].....	...	6.5	5.5	5.4	8.7	0.070 ± 0.002	27.1	9.0	169.1	9010 ± 90	SP	B, C	C II
	...	6.7	7.2	5.3	11.1	0.073 ± 0.003	25.4	8.9	146.8	8160 ± 40	TP	B, A	^{3}He
G49.486−0.38[e].....	W51	6.5	6.3	3.7	6.7	0.092 ± 0.004	82.2	60.0	489.8	7890 ± 20	SP	A, A	C II
	W51	6.5	6.3	4.1	7.5	0.084 ± 0.002	82.5	48.9	411.4	7240 ± 60	SP	C, A	^{3}He
G49.582−0.38.....	...	6.6	4.4	4.7	6.1	0.083 ± 0.005	6.6	2.9	91.3	1850 ± 90	TP	C, A	C II
G61.470+0.09.....	S88	7.6	2.4	0.4	0.3	0.066 ± 0.006	4.9	296.7	5391.6	9120 ± 60	SP	A, C	C II
G63.168+0.46.....	S90	8.0	1.5	4.7	2.0	0.074 ± 0.008	3.8	1.7	148.3	7370 ± 70	SP	B, A	^{3}He
G70.300+1.60.....	K3-50	9.8	8.5	3.9	9.6	0.103 ± 0.016	13.2	8.5	161.9	10,810 ± 130	SP	A, C	C II
G75.834+0.40.....	...	8.8	5.1	3.2	4.7	0.096 ± 0.006	9.0	8.7	223.1	8370 ± 50	SP	B, C	C II
G76.383−0.62.....	S106	8.4	0.7	2.1	0.4	0.081 ± 0.006	10.4	23.2	1352.2	12,930 ± 170	SP	A, D	C II
G79.293+1.30[e].....	DR 7	10.6	8.2	4.1	9.8	0.089 ± 0.005	10.0	5.7	127.0	9100 ± 70	SP	B, B	C II

TABLE 1—*Continued*

Source	Name	R_{Gal} (kpc)	d_{Sun} (kpc)	Θ_{diam} (arcmin)	D (pc)	$n(^4He^+)/n(H^+)$	S_ν (Jy)	T_C^B (K)	n_e (cm^{-3})	T_e^{*a} (K)	Mode[b]	QFs[c]	Survey
G79.293+1.30[e]	DR 7	10.6	8.2	4.8	11.4	0.099 ± 0.009	11.3	4.8	106.8	8220 ± 80	SP	C, B	^{3}He
G81.681+0.54	DR 21	8.5	2.2	2.2	1.4	0.068 ± 0.003	19.4	37.8	853.8	9120 ± 40	SP	A, A	C II
G93.060+2.81	...	12.3	8.5	...	...	0.068 ± 0.024	0.0	...	...	10,840 ± 270	TP	C, C	^{3}He
G102.88−0.72	S132	11.3	5.8	17.0	29.0	0.075 ± 0.035	7.8	0.3	17.3	14,800 ± 12,780	TP	E, E	^{3}He
G107.18−0.95	S142	10.6	4.3	10.7	13.4	0.052 ± 0.018	4.6	0.4	29.1	10,400 ± 270	TP	D, E	^{3}He
G110.11+0.04	S156	11.5	5.3	1.8	2.8	0.040 ± 0.010	1.7	5.4	232.6	9070 ± 140	SP	A, D	^{3}He
G111.53+0.82	S158/NGC 7538	12.4	6.4	4.8	8.8	0.089 ± 0.004	18.9	8.2	158.2	8230 ± 40	SP	B, A	^{3}He
G112.24+0.23	S162/NGC 7635	11.1	4.7	6.8	9.2	0.083 ± 0.015	3.4	0.7	46.1	8070 ± 130	SP	B, C	^{3}He
G118.15+4.96	S171 A	9.0	0.9	22.8	6.1	0.064 ± 0.012	24.7	0.5	46.4	9540 ± 1050	TP	C, C	^{3}He
G133.72+1.21	W3	11.7	4.1	3.1	3.7	0.075 ± 0.004	40.0	41.1	549.0	8380 ± 40	SP	B, A	^{3}He
G133.790+1.4	...	12.5	5.0	4.7	6.9	0.081 ± 0.011	14.1	6.2	157.1	8880 ± 120	SP	C, A	^{3}He
G150.59−0.95	S206	11.5	3.3	4.8	4.5	0.092 ± 0.008	5.8	2.5	125.0	9710 ± 90	SP	B, B	^{3}He
G151.587−0.2[d]	S209 N	16.7	8.7	5.6	14.1	0.081 ± 0.019	7.8	2.5	73.7	12,570 ± 360	SP	C, C	^{3}He
G151.59−0.23[d]	S209	16.9	8.9	5.6	14.4	0.078 ± 0.007	7.8	2.5	70.7	10,510 ± 90	SP	B, B	^{3}He
G151.636−0.5[d]	S209 S	19.9	12.0	5.6	19.5	0.079 ± 0.028	1.0	0.3	21.6	8680 ± 340	SP	B, E	^{3}He
G155.36+2.61	S212	16.7	8.6	5.8	14.4	0.117 ± 0.023	2.1	0.6	35.5	10,460 ± 240	SP	B, D	^{3}He
G169.19−0.90	S228	13.8	5.3	4.8	7.4	0.065 ± 0.028	1.0	0.4	40.3	9700 ± 740	SP	B, E	^{3}He
G173.60+2.80	S235	10.1	1.6	6.6	3.1	0.049 ± 0.010	3.3	0.7	81.6	8940 ± 170	SP	A, D	^{3}He
G189.97+0.40	S252	12.1	3.6	12.1	12.8	0.055 ± 0.017	5.2	0.3	27.6	9460 ± 230	TP	C, E	^{3}He
G201.6+1.6	...	12.7	4.4	10.9	14.0	0.078 ± 0.021	4.1	0.3	26.1	9140 ± 220	SP	C, D	^{3}He
G206.122−2.3[d]	Rosette B	10.7	2.4	10.0	6.9	0.061 ± 0.019	2.8	0.3	32.3	7480 ± 210	TP	D, D	^{3}He
G206.618−1.8[d]	Rosette A	10.5	2.2	18.0	11.6	0.069 ± 0.021	14.0	0.4	32.9	10,770 ± 310	TP	D, D	^{3}He
G209.01−19.4	Ori A	8.9	0.5	5.5	0.8	0.078 ± 0.005	258.5	83.9	1672.6	7860 ± 40	TP	A, B	^{3}He
G213.71−12.6	MONR 2	9.6	1.3	1.2	0.5	0.070 ± 0.002	5.7	40.5	1567.9	8570 ± 90	SP	A, D	^{3}He
G220.508−2.8	S291	16.6	9.2	9.4	25.2	0.070 ± 0.002	2.0	0.2	18.0	21,810 ± 4670	SP	C, E	^{3}He
G223.7−1.9	...	9.7	1.6	14.8	6.7	0.070 ± 0.002	6.1	0.3	34.2	9910 ± 1770	SP	C, E	^{3}He
G227.79−0.12	S298/NGC 2359	12.4	5.0	10.6	15.3	0.099 ± 0.050	3.5	0.3	25.4	13,560 ± 770	SP	A, E	^{3}He
G231.48−4.40	RCW 6	12.9	5.8	9.0	15.1	0.087 ± 0.020	3.7	0.4	28.9	9740 ± 260	SP	B, D	^{3}He
G243.16+0.37	S311	12.0	5.4	10.2	16.0	0.080 ± 0.009	14.5	1.4	49.9	10,220 ± 110	SP	B, B	^{3}He
G345.03+1.54	...	7.1	...	10.8	...	0.070 ± 0.002	7.7	0.6	...	6850 ± 350	SP	D, D	C II
G345.23+1.03	...	7.3	...	4.4	...	0.030 ± 0.002	8.8	4.4	...	7590 ± 120	SP	B, E	C II
G345.31+1.47	...	7.1	...	7.3	...	0.059 ± 0.004	13.4	2.4	...	8530 ± 640	SP	B, C	C II
G345.40+1.41	...	7.0	...	...	...	0.059 ± 0.004	...	...	...	... ± ...	...	B, D	C II
G345.43−0.94	...	6.2	14.0	3.2	13.0	0.059 ± 0.002	27.5	26.5	228.4	6960 ± 50	SP	A, A	C II
G345.54+0.10	...	9.4	17.5	3.9	19.9	0.070 ± 0.002	1.6	1.0	40.3	12,320 ± 970	SP	C, E	C II
G347.96−0.44	...	2.5	...	5.7	...	0.070 ± 0.002	2.3	0.7	...	5930 ± 200	SP	B, D	C II
G348.23−0.98	...	6.3	14.3	3.3	13.6	0.182 ± 0.016	8.3	7.6	118.6	6610 ± 100	SP	A, C	C II
G348.72−1.03	...	6.9	...	4.3	...	0.062 ± 0.004	32.0	17.3	...	7150 ± 90	SP	B, B	C II
G350.13+0.09	...	2.6	6.2	3.1	5.5	0.072 ± 0.005	6.1	6.4	171.7	6710 ± 120	SP	B, D	C II
G351.063+0.6	...	7.9	0.6	8.0	1.4	0.070 ± 0.002	26.2	4.0	283.3	10,570 ± 340	SP	C, D	C II
G351.192+0.7	...	8.8	17.1	7.4	36.9	0.049 ± 0.003	30.6	5.4	59.3	5610 ± 20	SP	B, A	C II
G351.201+0.4	...	7.2	1.4	6.8	2.7	0.081 ± 0.007	15.9	3.4	178.5	6650 ± 70	SP	B, C	C II
G351.246+0.7[d]	NGC 6334 A	8.8	17.1	5.6	27.7	0.052 ± 0.005	36.2	11.4	106.1	8560 ± 70	TP	C, B	^{3}He
G351.358+0.6	S8	7.9	0.6	7.0	1.3	0.067 ± 0.002	54.4	10.9	460.7	6840 ± 40	SP	C, A	C II
G351.368+0.7[d]	NGC 6334 D	7.9	16.2	7.5	35.2	0.058 ± 0.004	61.8	10.9	94.0	9700 ± 90	TP	C, A	^{3}He
G351.467−0.4	...	5.1	3.4	3.5	3.4	0.070 ± 0.002	2.8	2.3	133.2	7460 ± 120	SP	B, C	C II
G351.613−1.2	...	6.0	14.3	2.9	12.2	0.088 ± 0.005	23.2	26.3	238.2	7620 ± 30	SP	A, A	C II
G351.64−1.26	...	6.1	...	3.1	...	0.083 ± 0.004	21.0	21.5	...	6490 ± 210	SP	B, B	C II
G351.69−1.17	...	6.4	14.7	5.1	22.0	0.077 ± 0.007	11.8	4.4	72.2	7560 ± 90	SP	B, B	C II
G352.61−0.17	...	2.0	6.7	4.1	8.0	0.070 ± 0.002	2.6	1.5	70.3	7560 ± 240	SP	B, C	C II
G353.035+0.7	...	6.8	1.7	3.7	1.8	0.116 ± 0.008	7.1	5.2	260.2	5630 ± 40	SP	B, C	C II
G353.08+0.36	...	7.9	0.6	9.5	1.8	0.078 ± 0.009	19.4	2.1	168.3	5390 ± 100	SP	E, C	C II
G353.14+0.66	...	7.6	16.0	7.2	33.5	0.096 ± 0.006	56.1	10.6	88.7	6250 ± 30	SP	B, B	C II
G353.186+0.8	S11	7.6	0.9	5.2	1.3	0.107 ± 0.004	66.3	23.7	682.4	7100 ± 40	SP	B, B	C II
G353.21+0.91	...	7.7	...	5.0	...	0.099 ± 0.004	62.1	23.8	...	6900 ± 50	SP	B, B	C II
G353.398−0.3	...	5.2	3.3	2.6	2.5	0.050 ± 0.006	9.3	13.2	376.7	8480 ± 60	SP	A, C	C II
G353.43−0.37	...	5.3	3.3	2.7	2.5	0.064 ± 0.011	8.6	11.8	350.7	7750 ± 110	SP	B, C	C II

[a] The electron temperatures were rounded off to the nearest 10 K.
[b] Mode refers to the continuum observing mode, where "TP" denotes total power and "SP" denotes switched power observations.
[c] QFs correspond to the continuum and line quality factors, respectively.
[d] M16, M17, NGC 6334, Rosette, and S209 were observed at different positions in the ^{3}He survey.
[e] Observed in both C II and ^{3}He surveys.

many conditions, LTE is a good approximation and the LTE electron temperature T_e^* is close to T_e.

For conditions close to LTE and where pressure broadening is not significant, the β/α RRL intensity ratio should be about 0.28, and the β/α RRL line width ratio should be close to 1 (Shaver & Wilson 1979). We determined these ratios for the ^{3}He survey where the H114β line has been observed. For our best QF data (28 objects), the average intensity ratio is 0.26 ± 0.03 and the average line width ratio is 1.02 ± 0.06. Moreover, Shaver (1980) defined a RRL observing frequency, $\nu_{\rm LTE}$, such that $T_e^* = T_e$. This optimal RRL frequency is a function of emission measure: $\nu_{\rm LTE} \sim 0.081\ {\rm EM}^{0.36}$. It is essentially independent of density, temperature, or structure within the nebula. Using our best QF data (88 objects), we obtain an average frequency $\nu_{\rm LTE} = 6.9 \pm 3.6$ GHz. This is close to our observing frequency of 8.584 GHz. Furthermore, detailed density structure models for a subset of our ^{3}He survey nebulae were made using high-resolution Very Large Array (VLA) radio continuum images and high-order RRLs that were sensitive to local electron densities (Balser et al. 1999). The non-LTE electron temperatures calculated for these models are very close to the LTE electron temperature determined using the H91α lines. We therefore conclude that our LTE electron temperature must be very close to the real average nebular electron temperature.

3.2. *Nebular Angular Size*

We derived the H II region angular sizes by assuming homogeneous, spherical nebulae. Each nebula has an observed full width at half-maximum size of $\Theta_{\rm src} = [\Theta({\rm R.A.})\Theta({\rm Decl.})]^{1/2}$ (geometric mean; see Quireza et al. 2006). Assuming that the source has a Gaussian brightness distribution and that the telescope beam has a Gaussian pattern with half-power beam width (HPBW), then $\Theta_{\rm src}$ is

$$\Theta_{\rm G} = \sqrt{\left(\Theta_{\rm src}^2 - {\rm HPBW}^2\right)}, \quad (3)$$

where $\Theta_{\rm G}$ is the nebular Gaussian angular size (Mezger & Henderson 1967). We use the technique developed by Panagia & Walmsley (1978) to derive $\Theta_{\rm diam}$, the angular size of a homogeneous, spherical nebula from $\Theta_{\rm G}$. We use TP continuum measurements if at all possible. The nebular $\Theta_{\rm diam}$ so derived is listed in Table 1 together with the linear diameter, D. Objects whose angular sizes are close to the telescope HPBW are not well resolved and consequently have less precise estimates for their sizes. This will give a larger error for any physical property whose derivation depends on the angular size. One important property that requires precise angular size measurements is the electron density.

3.3. *rms Electron Density*

If a homogeneous, spherical nebula is also optically thin, then the electron density can be calculated from the peak continuum brightness temperature of the source, T_C^B (Balser 1995):

$$n_e = \left[\frac{T_C^B \nu^2 (T_e^*)^{1/2}}{8.77 \times 10^{-3}\ \ln(X)\Theta_{\rm diam} d_{\rm Sun}}\right]^{1/2} {\rm cm}^{-3}, \quad (4)$$

where ν is the frequency (8.66565 GHz), T_e^* is the electron temperature in K, $X = 4.954 \times 10^{-2}\ (T_e^*)^{3/2}/\nu$, $\Theta_{\rm diam}$ is the spherical size in arcminutes, and $d_{\rm Sun}$ is the source's distance, in kpc, from the Sun (see § 6). Here we assume no doubly ionized helium gas within the H II region. The flux density, S_ν, is

$$S_\nu = 1.223 T_C^B \left(\frac{\Theta_{\rm diam}}{\lambda}\right)^2 = 2.647 \left(\frac{T_C}{\eta_b}\right)\left(\frac{\Theta_{\rm src}}{\lambda}\right)^2 {\rm Jy}, \quad (5)$$

where temperatures are in K, angular sizes are in arcminutes, and the wavelength is in cm. The beam efficiency of the NRAO 140 Foot telescope is $\eta_b = 0.86$.

The nebular flux and electron densities calculated in this way are listed in Table 1. Because T_C^B measures the continuum radiation produced by free-free thermal bremsstrahlung in the plasma, its value depends on the integral of n_e^2 along the line of sight. Thus, the electron densities derived here are the rms density of the entire H II region. If the nebula is homogeneous, then the rms electron density equals the local density. Detailed analysis, however, shows that this is not generally true for Galactic H II regions (Osterbrock & Flather 1959). The rms densities are probably somewhat lower than the true densities of the emitting regions, since the gas is not evenly distributed throughout the H II region (Fich & Silkey 1991).

3.4. *Comparison with Previous Studies*

Here we compare our electron temperatures with results from the literature for nebulae in our sample. The majority of these previous efforts were also studying the Milky Way T_e gradient. Most T_e estimates come from RRLs, although measurements in other spectral regions are available for a limited number of objects. We summarize the T_e differences in Table 2, which lists the number of sources in common, N, the average percentage difference between our results and the reference, and the average percentage of the absolute value of difference between our results and the reference. The average difference will reveal any offset in T_e scales; the average absolute value difference measures the scatter between the studies. The table also lists the type of observation and the method used to calculate T_e (line-to-continuum ratio, optical forbidden lines, radio continuum emission, etc.).

It is immediately apparent that our values of T_e are systematically high compared with previous studies. While one might expect systematic differences between values of T_e determined by different methods, the largest offsets are found between our values and those of Wink et al. (1983, hereafter WWB83) and Shaver et al. (1983, hereafter SMNDP83), which are both RRL studies similar to ours, with many sources in common. In Figure 1 we compare our LTE electron temperatures with their values of T_e. Our best QF data (A, B, and C) are plotted as filled symbols. Our values are systematically 11% higher than WWB83 and 13% higher than SMNDP83.

We considered the origin of these differences in some detail. Any term in equation (1) may be the explanation. There may also be issues of calibration between line and continuum measurements and between telescopes. All the RRL studies were made at different frequencies, using different telescopes with correspondingly different beam sizes. Thus, each survey probes different volumes of each nebula. Certainly, there is complex structure inside some H II regions, which includes large density and temperature fluctuations. The T_e derived from disparate RRL transitions using different telescopes can certainly be different, especially under the assumption of LTE.

The beam size for the WWB83 study was substantially smaller than ours, so on average, they were observing higher density gas than we did. Exactly how to interpret this is quite complex and would require detailed density and excitation modeling for each

TABLE 2
AVERAGE DIFFERENCES IN ELECTRON TEMPERATURE DETERMINATIONS

Reference	N	$100\langle(\mathrm{Us}-\mathrm{Ref})/\mathrm{Us}\rangle$	$100\langle\mathrm{abs}(\mathrm{Us}-\mathrm{Ref})/\mathrm{Us}\rangle$	Observation	Method
PTR78	2	3.6	12.9	Optical	[O III] $\lambda\lambda$4363, 5007
WBW79	6	3.6	4.9	RRL	$T_L(\mathrm{H66}\alpha)/T_C$
TMP80	7	2.9	4.7	RRL	$T_L(\mathrm{H66}\alpha)/T_C$
	5	2.7	11.0	RRL	$T_L(\mathrm{H76}\alpha)/T_C$
GR83	3	9.3	11.1	RRL	$T_L(\mathrm{H125}\alpha)/T_C$
WWB83	30	10.9	14.4	RRL	$T_L(\mathrm{H76}\alpha)/T_C$
SMNDP83	17	13.3	14.2	RRL	$T_L(\mathrm{H109}\alpha)/T_C$
ACA96	4	4.5	15.8	RRL	$T_L(\mathrm{H66}\alpha, 76\alpha, 93\alpha)/T_C$
BBRW99	16	−0.2	6.7	RRL	$T_L(\mathrm{H91}\alpha)/T_C$
DPCC00	2	9.8	9.8	Optical	[O III] $\lambda\lambda$4363, 5007
OCAR02	2	5.3	8.7	Radio	Continuum
EGPPRR05	3	5.1	5.1	Optical	[O III], [S III], [Ar III]
	3	−1.2	5.5	Optical	[O II], [N II]

NOTE.—QF = A, B, and C, without the outlier G49.582−0.38.

REFERENCES.—ACA96: Afflerbach et al. 1996; BBRW99: Balser et al. 1999; DPCC00: Deharveng et al. 2000; EGPPRR05: Esteban et al. 2005; GR83: Garay & Rodríguez 1983; OCAR02: Omar et al. 2002; PTR78: Peimbert et al. 1978; SMNDP83: Shaver et al. 1983; TMP80: Thum et al. 1980; WBW79: Wilson et al. 1979; WWB83: Wink et al. 1983.

nebula. The continuum measurement technique is also important. These details can lead to T_C measurements that are too low (the continuum data do not extend beyond the H II region) or too high (Galactic nonthermal continuum is included in T_C).

In Balser et al. (1999), our continuum observations from the NRAO 140 Foot telescope, the Max-Planck-Institut für Radioastronomie (MPIfR) 100 m telescope, and the VLA were carefully cross-calibrated, confirming the calibration techniques used for the ^{3}He and C II surveys. Furthermore, our recombination line data are vastly superior to these previous studies due to a combination of improved technology (system temperatures of ∼35 K compared with ∼100 K) and longer integration times (tens of hours compared with tens of minutes). In summary, we have yet to identify just why WWB83 and SMNDP83 have lower T_e values.

We have reason to believe that our electron temperatures are the best values derived to date. We have substantially better recombination line data that have unsurpassed sensitivity due to a combination of modern receivers and our extremely long integration times. The modes of the distributions of source integration times for the carbon and ^{3}He surveys are ∼15 and ∼50 hr, respectively. Previous efforts have source integration times of ∼30 minutes or less. Finally, these extremely high signal-to-noise ratio spectra allow us to model the spectral baseline frequency structure with unprecedented accuracy, which gives us great confidence in our determination of the recombination line parameters.

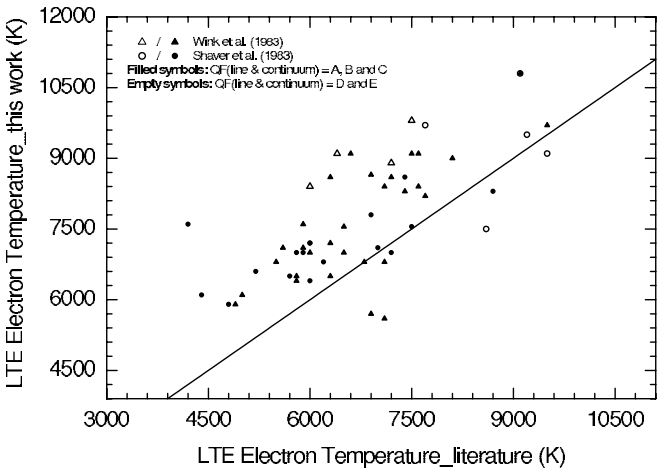

FIG. 1.—Nebular LTE electron temperatures derived here, compared with those from SMNDP83 (*circles*) and WWB83 (*triangles*) for objects in common. Filled symbols denote our highest quality data (QFs *A*, *B*, and *C*); open symbols flag our poorer quality data. The locus of T_e (us) = T_e (literature) is shown by the solid line.

4. NEBULAR DISTANCES

We derived the Galactocentric distance, R_{Gal}, for each nebula, using the observed recombination line LSR (local standard of rest) velocity and assuming a Galactic rotation curve. For sources located inside the solar orbit, we used the Clemens (1985) rotation curve; otherwise, the Brand & Blitz (1993) rotation curve was used. Both rotation curves assume purely circular rotation laws, and they place the Sun at a Galactocentric distance of $R_0 = 8.5$ kpc orbiting the Galactic center at an LSR circular velocity of $\Theta_0 = 220$ km s^{-1}. The nebular RRL velocities can be found in Table 2 of Quireza et al. (2006). Here we have thus chosen to use only these kinematic determinations of the R_{Gal} of our sources. Many of the previous studies of the Milky Way T_e gradient have used a mix of techniques to establish the nebular R_{Gal}.

The nebular heliocentric distance, d_{Sun}, is also listed in Table 1. These distances were also derived kinematically from the observed nebular LSR velocity. For sources located inside the solar orbit, each radial velocity value corresponds to two distances (the "near" and "far" kinematic distances) equally spaced on either side of the tangent point. In most cases, we were able to resolve the kinematic distance ambiguity by measuring the 21 cm H I absorption spectrum toward the nebular continuum. Discrimination between the near and far distance was done by comparing the maximum velocity of the H I absorption with that of the H II region recombination line. For those objects for which we could not resolve the ambiguity via H I absorption, we used distances available in the literature. Our H I survey, observational technique, method of analysis, and detailed description of our d_{Sun} derivations are described by C. Quireza et al. (2006, in preparation).

Figure 2 shows the distribution of our H II region sample projected onto the Galactic plane. Only sources with known d_{Sun} are plotted. The majority of our H II regions are located in the first and fourth Galactic quadrants, and their R_{Gal} values can reach ∼19 kpc. Some sources are located beyond the Galactic center, with $d_{\mathrm{Sun}} \sim 20$ kpc. Different symbols identify the ^{3}He (*triangles*)

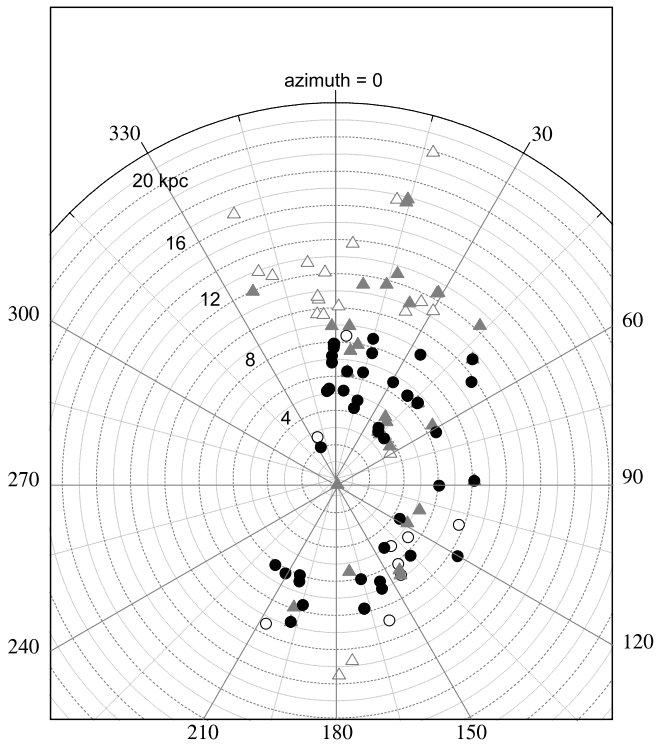

FIG. 2.—Distribution of the H II region sample projected onto the Galactic plane, plotted as a function of Galactocentric radius and azimuth. Different symbols identify the ^{3}He (*triangles*) and C II survey (*circles*) nebulae. Filled/open symbols have the same meaning as in Fig. 1.

and C II survey (*circles*) nebulae. The ^{3}He sources span a larger range of Galactocentric radius and azimuth than do the C II nebulae. Filled symbols denote our highest QF sources (QFs *A*, *B*, and *C*); open symbols flag our poorer quality data. Unfortunately, many of the low-QF objects are astrophysically significant; they are located in areas of the disk not well covered by nebulae with more accurate data.

There is a good reason for using only kinematic distances: homogeneity of approach. A detailed comparison between optical and kinematic distances is beyond the scope of this paper. Both approaches have their limitations, and perhaps the resolution will be a direct trigonometric measurement using very long baseline interferometry (VLBI) techniques, which is being pioneered by Mark Reid and his team (Xu et al. 2006; Hachisuka et al. 2006).

It is common to cite optical spectrophotometric distance uncertainties to be of order 15%. But as one delves into the literature in detail, one finds a greater dispersion. For any given analysis, the 15% holds, but slight differences in spectral classification, adopted luminosity scale (which is model-atmosphere-dependent), and uncertainties in the extinction correction conspire to give a larger uncertainty when different research groups measure the distances to the same object. These systematic errors are the optical counterpart of the streaming motion uncertainty inherent in kinematic distances. Thus, the consistency of optical distances may not be all that much better than the dispersion between optical and radio distances. Most of our H II regions are not optically visible. A quick internet search for the seven most distant (in $R_{\rm Gal}$) nebulae shows that the mean absolute value of the radio-optical discrepancy for these sources is $11\% \pm 6\%$.

Noncircular streaming motions will certainly affect the kinematically derived distances. If we knew what the Galactic-scale streaming motions are, we would certainly correct for them. The Galactic bar, the spiral density wave, accretion events such as the Sgr dwarf elliptical galaxy, and close encounters such as that which occurred for the Large Magellanic Cloud (LMC) will all generate large-scale, asymmetric streaming motions in the Milky Way disk. At present, there is no way to calculate these effects accurately and thus generate the true velocity field of the Galaxy.

5. ELECTRON TEMPERATURE GRADIENT

5.1. *Gradient Magnitude*

Our H II region sample contains some sources observed in both the ^{3}He and C II surveys, as well as nebulae that have RRL spectra taken toward multiple positions. For sources common to both surveys,[7] the T_e^* and $R_{\rm Gal}$ values derived for the ^{3}He and C II surveys were averaged (simple mean). These nebulae do *not* appear twice in the analysis of the electron temperature gradient. We only averaged data of good QFs (*C* or better) that also were in good agreement. (The origin of some differences between the two surveys is discussed by Quireza et al. 2006.) These T_e^* values are consistent with each other within the errors; differences are not larger than $\sim$10%.

In the ^{3}He survey, five morphologically complex H II regions had spectra taken toward two or three different positions. These nebulae are G16.936+0.75 (the brightest and northernmost components: M16 and M16 N), M17 (northernmost and southernmost components: M17 N and M17 S), NGC 6334 (NGC 6334 A and NGC 6334 D), Rosette (Rosette A and Rosette B), and S209 (brightest, northernmost, and southernmost components: S209, S209 N, and S209 S). Because these nebulae are extended objects with angular diameters larger than the 3.′20 HPBW beam size, each of the observed components is included in our analysis of the T_e^* gradient. Since these components are separated by more than a beam width, any T_e^* differences within an object are real temperature fluctuations.

Figure 3 shows our nebular LTE electron temperatures, T_e^*, plotted as a function of the Galactocentric distance, $R_{\rm Gal}$. We include only the 78 sources with our best data (QFs *A*, *B*, and *C*: sample B described below) for both line and continuum. Least-squares linear fits to the gradient, $T_e^* = a_1 + a_2 R_{\rm Gal}$ K, are shown for the entire sample and, separately, for nebulae located inside and outside the solar orbit. The gradient is flatter for H II regions in the inner Milky Way.

Seven nebulae in Figure 3 are flagged because they do not follow the general T_e^* gradient. Two nebulae, G49.582−0.38 (1851 K, 6.5 kpc) and G5.956−1.265 (3416 K, 7.8 kpc) have temperatures much lower than the 7585 ± 1262 K average T_e^* for the 6–8 kpc interval of $R_{\rm Gal}$. Moreover, the G49.582−0.38 temperature is $\sim$3600 K lower than the WWB83 value. For these sources, we had to use TP continuum measurements to derive T_e^*. This may have compromised the accuracy of our result. G5.899−0.427 (11,128 K, 6.1 kpc) also lies far from the general trend of the sample. Here, however, we do not have any reason to suspect that its T_e^* derivation is less reliable than that of other sources in the 6–8 kpc zone.

The four remaining anomalous nebulae are located at the extremes of the $R_{\rm Gal}$ distribution of our H II region sample. These nebulae thus have a large influence on the temperature gradient fits. The two Galactic center sources, G1.13−0.1 (7135 K, 0.1 kpc) and Sgr B2 (8169 K, 0.4 kpc), may indeed share the anomalous chemical abundances in this region (see § 6.2). The two outer Galaxy sources, S209 (10,506 K, 16.9 kpc) and S209 N (12,565 K, 16.7 kpc), are part of the same H II region. Here again we can identify no compelling reason to exclude these nebulae.

[7] G16.936+0.75 (M16), G23.421−0.21, G25.382−0.17 (3C 385), G43.169+0.0 (W49), G49.384−0.29, G49.486−0.38 (W51), and G79.293+1.29.

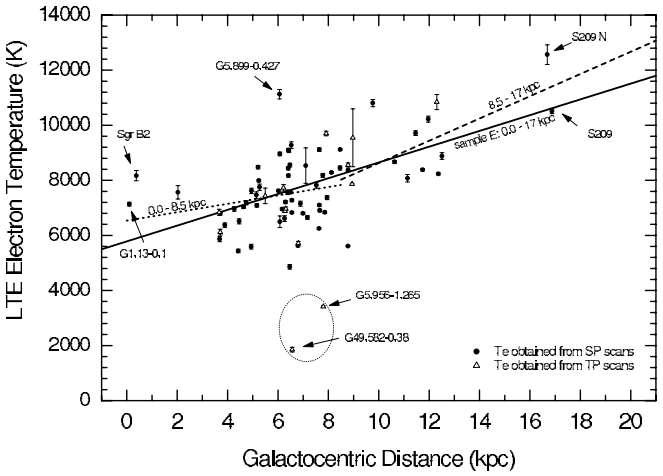

FIG. 3.—Nebular LTE electron temperature plotted as a function of the Galactocentric distance for the best data (QFs *C* or better: sample B in Table 3). Least-squares linear fits to the gradient for the entire sample and, separately, for nebulae located inside and outside the solar orbit are shown. The gradient is flatter for H II regions in the inner Milky Way.

We analyzed six subsets of our H II region sample in order to assess the effects of sample selection on the temperature gradient.[8] Sample A includes all 109 of our sources. Sample B includes only high-QF sources (the 78 sources shown in Fig. 3 that have QFs of *C* or better). Sample C removes TP continuum sources from sample B, for a total of 64 nebulae. Sample D removes the seven sources flagged in Figure 3 from Sample B, for a total of 71 nebulae. Sample E removes G49.582−0.38 and G5.956−1.265 from sample B, for a total of 76 nebulae. Sample F removes three sources from sample E (the two Galactic center sources and G5.899−0.427), for a total of 73 nebulae.

We fit least-squares linear temperature gradients to each sample. The fit results are summarized in Table 3, which lists the coefficients a_1 and a_2 and their standard deviations $\sigma(a_1)$ and $\sigma(a_2)$, together with the correlation coefficient r, the χ^2 of the fit, the number N of sources in the sample, and the $R_{\rm Gal}$ range of the sample, $\Delta R_{\rm Gal}$. In all cases, the gradient is close to 300 K kpc^{-1}. Even our smallest sample of 64 objects is astrophysically significant in the sense that it spans a large range of Galactic radius. The fit to the sample E nebulae is shown as a solid line in Figure 3. *Unless otherwise stated, we use the sample E gradient fit in all subsequent analysis described herein*. This fit is $T_e = (5780 \pm 350) + (287 \pm 46)\ R_{\rm Gal}$ ($r = 0.59$, $N = 76$).

Figure 3 shows T_e^* error bars. Many nebulae have error bars that are smaller than the plotted symbols. The error bars shown are the propagated statistical errors in the measured quantities. Various systematic effects almost certainly lead to uncertainties larger than the error bars shown. Because systematic errors are inherently unquantifiable and certainly are not normally distributed, any attempt to plot "systematic error bars" would be misleading.

This is especially true for errors in the kinematically determined $R_{\rm Gal}$. They are entirely dominated by systematic effects,

[8] G345.40+1.41, S291, and S132 were excluded from all samples. We have no continuum information for G345.40+1.41. The other nebulae have large uncertainties associated with either their line or continuum data.

TABLE 3

T_e^* GRADIENT FITS: $T_e^* = a_1 + a_2 R_{\rm Gal}$

Sample	a_1 (K)	a_2 (K kpc^{-1})	r	χ^2	N	$\Delta R_{\rm Gal}$ (kpc)
A[a]	5840 ± 410	281 ± 49	0.49	1690	109	0.0–20.0
B[b]	5660 ± 430	286 ± 56	0.50	1430	78	0.0–17.0
C[c]	5960 ± 380	261 ± 50	0.56	1199	64	0.0–17.0
D[d]	5480 ± 410	312 ± 55	0.56	1053	71	2.0–13.0
E[e]	5780 ± 350	287 ± 46	0.59	1173	76	0.0–17.0
F[f]	5300 ± 350	340 ± 45	0.67	1059	73	2.0–17.0
		$R_{\rm Gal} < R_0$				
A[a]	6110 ± 690	222 ± 110	0.23	1675	75	0.0–8.5
B[b]	6750 ± 660	89 ± 106	0.11	1430	62	0.0–8.5
C[c]	6750 ± 550	124 ± 90	0.19	1139	52	0.0–8.5
D[d]	5730 ± 600	268 ± 96	0.35	1007	57	2.0–8.5
E[e]	6540 ± 520	153 ± 85	0.23	1130	60	0.0–8.5
F[f]	5730 ± 600	268 ± 96	0.35	1007	57	2.0–8.5
		$R_{\rm Gal} > R_0$				
A[a]	7190 ± 1370	182 ± 115	0.27	1733	34	8.5–20.0
B[b]	4590 ± 1510	404 ± 130	0.64	1279	16	8.5–17.0
C[c]	3780 ± 1910	453 ± 157	0.67	1357	12	8.5–17.0
D[d]	5220 ± 2550	342 ± 239	0.38	1305	14	8.5–13.0
E[e]	4590 ± 1510	404 ± 130	0.64	1279	16	8.5–17.0
F[f]	4590 ± 1510	404 ± 130	0.64	1279	16	8.5–17.0

[a] All QFs: 106 sources, plus six additional pointings within five of those sources. S291 and S132 were not included due to their large errors; we have no continuum for G345.40+1.41.
[b] QF = *A*, *B*, and *C*.
[c] Sample B, excluding sources calculated with only TP continuum.
[d] Sample B, excluding outlying values of T_e^* flagged in Fig. 3.
[e] Sample B, excluding the outliers G49.582−0.38 and G5.956−1.265.
[f] Sample E, excluding Sgr B2, G1.13−0.1, and G5.899−0.427.

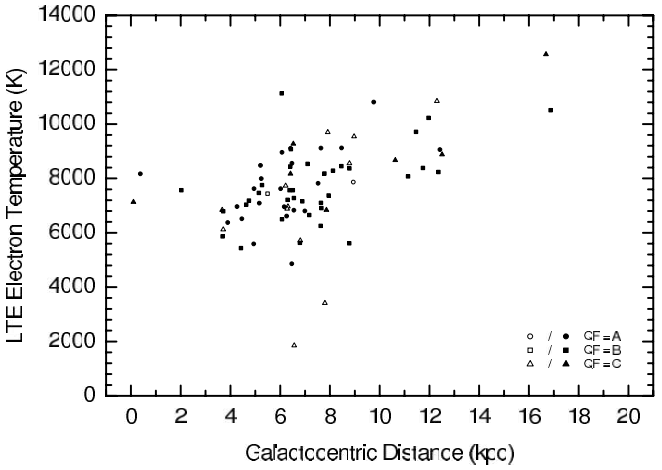

FIG. 4.—Same as Fig. 3, but showing the quality factor of the continuum data. Filled symbols denote T_e^* temperatures derived from SP continuum measurements; open symbol sources used TP measurements.

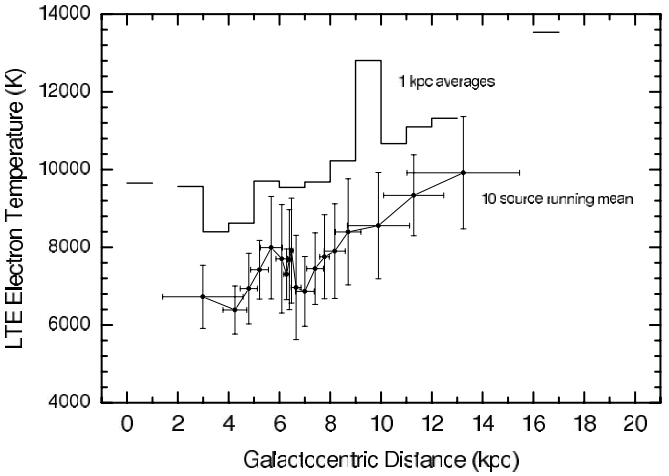

FIG. 5.—"Smoothed" electron temperatures plotted as a function of Galactocentric distance, $R_{\rm Gal}$. Symbols with error bars are a 10 point running mean of T_e^* and $R_{\rm Gal}$, drawn at intervals of four points along $R_{\rm Gal}$. Horizontal line segments show the mean T_e^* in each 1 kpc wide $R_{\rm Gal}$ interval. These are offset by +2000 K for clarity. Both smoothing algorithms suggest a slightly smaller gradient in the inner Galactic disk.

including Galactic-scale streaming motions, and differences in the choice of rotation curve. Estimates for the magnitude of the error of the $R_{\rm Gal}$ determination are typically ~25% (e.g., Kuchar & Bania 1990). This value is the quadrature sum of the ~15% error due to the uncertainty in the rotation curve and of the ~20% error due to streaming/noncircular motions. Here we have, however, at least made the $R_{\rm Gal}$ determinations in a uniform, systematic way that distinguishes this effort from the majority of T_e gradient studies, which normally draw their distances from a heterogeneous mixture of techniques.

It is important to understand the nature of the scatter in Figure 3. Deharveng et al. (2000) argued that a significant fraction of the scatter in earlier investigations of the electron temperature gradient may result from observational errors and sample inhomogeneity. They cited the case of the bright H II region S206: the electron temperature estimated by various authors ranges from $\leq$8000 K (Churchwell et al. 1978; Mezger et al. 1979) to about 13,000 K (Lichten et al. 1979). In our study sample, homogeneity is not a problem, and the statistical errors are quite small compared to the scatter in T_e^*.

Could systematic error be responsible for the scatter? We believe that the main source of systematic error arises from determining the baseline level of our continuum measurements. The continuum QFs give at least a qualitative estimate of this. In Figure 4 we plot the Figure 3 points without error bars and use different symbols to identify the continuum QFs. The two lower outliers are indeed QF = *C*, but for the bulk of the points, the differing QFs yield a comparable scatter. *From this, we conclude that the scatter in the points indicates a real spread in* T_e^*. That is, the dispersion in T_e^* at any $R_{\rm Gal}$ is indicative of intrinsic variations in T_e^* between nebulae.

5.2. *Electron Temperature Variations in Galactic Radius*

Given the size, uniformity, and precision of our sample, we can investigate whether there is more complex behavior than a linear gradient in the variation of T_e^* with $R_{\rm Gal}$. To reduce the scatter to make trends more visible, we have "smoothed" the data in two ways, as shown in Figure 5. The symbols with error bars are a 10 point running mean of T_e^* and $R_{\rm Gal}$ plotted at intervals of 4 points along the Galactocentric distance. The horizontal line segments show the mean T_e^* in each 1 kpc interval, ranging from $R_{\rm Gal} = 0-1$ kpc to 16–17 kpc. These are offset by +2000 K for clarity. Both techniques smooth the data in slightly different ways, and both suggest a slightly smaller gradient in the inner area of the Galactic disk.

We also made a least-squares second-order polynomial fit to the electron temperature gradient for the sample E sources. This fit was very similar to the best linear fit and perhaps even misleading because of the effect of the radial outliers. We therefore divided sample E sources into nebulae inside and outside the solar orbit and then fit two linear segments to these data subsets. These fits are shown in Figure 3. The slope interior to $R_{\rm Gal}$ is less than that in the outer Galaxy: 153 ± 85 K kpc^{-1} compared to 404 ± 130 K kpc^{-1}. This result is strongly influenced by the outliers. If we exclude G1.13−0.1, G5.899−0.427, Sgr B2, and S209 from the linear fits, we have a gradient of 268 ± 96 K kpc^{-1} for $R_{\rm Gal} < R_0$ and 342 ± 239 K kpc^{-1} for $R_{\rm Gal} > R_0$. We conclude that our data do not justify anything more elaborate than a single linear fit. The data do hint at more complex behavior, but a larger sample of nebulae at both very small and very large $R_{\rm Gal}$ is needed to explore it. This is to be expected, since our nebular sample was not chosen to study the disk electron temperature gradient. Indeed, having more nebulae at larger Galactocentric distances would significantly improve the determination of the electron temperature gradient. We in fact intend to make observations of more nebulae at larger $R_{\rm Gal}$ in the future because of this.

5.3. *Electron Temperature Variations in Galactic Azimuth*

In § 5.1 we conclude that the scatter in T_e^* at a given $R_{\rm Gal}$ is not due to observational error. Figure 6 shows a histogram of the percentage deviation of the nebular T_e^* from the best T_e gradient model fit to sample E. The deviations are Gaussian distributed with a $\Delta T_e/T_e$ dispersion of about 14%. This implies that Galactic H II regions have intrinsic T_e^* fluctuations of ~1100 K at any $R_{\rm Gal}$. SMNDP83 also argued that most of their scatter in T_e is intrinsic. Their Figure 17 shows that a realistic range in the effective temperature of the exciting stars (30,000–45,000 K) or of the electron density can account for a spread of T_e as large as 2000 K; this is confirmed by photoionization models (Rubin 1985; see § 6.1).

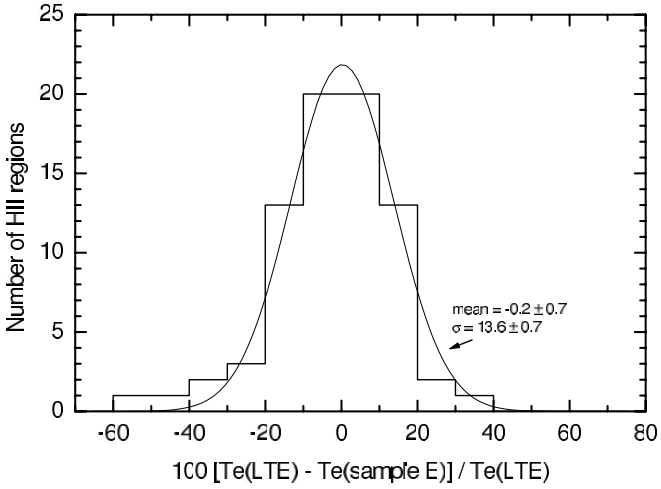

FIG. 6.—Histogram of the fractional deviation of the nebular electron temperature from the best temperature gradient model fit to sample E. The deviations are well fitted by a Gaussian distribution whose dispersion (σ) corresponds to an intrinsic electron temperature fluctuation of $\sim$1100 K at any Galactic radius.

Maps of radio continuum emission (Altenhoff et al. 1979; Reich et al. 1990; Fürst et al. 1990; Haynes et al. 1978) and our own continuum observations show that many H II regions are found spatially close to one another. The gas within a given complex of nebulae could share the same nucleosynthetic history, perhaps including self-enrichment. The nucleosynthetic history might, however, vary significantly from complex to complex. We searched our H II region sample for spatially clumped clusters of nebulae with similar T_e^* values and found no obvious signature of patchy nucleosynthesis.

Another possibility is that the assumption of axial symmetry in the stellar production of heavy elements is invalid. If the radial gradient were a function of Galactocentric azimuth, then the scatter in a T_e^* versus $R_{\rm Gal}$ Figure 3 type plot would result from lumping together nebulae from different azimuths into the same $R_{\rm Gal}$ bin. We have therefore searched for azimuthal differences in our nebular sample.

Figure 7 shows the nebular electron temperature plotted as a function of Galactocentric radius for four distinct ranges of Galactocentric azimuth. A difficulty in the analysis of the azimuthal variation of the temperature gradient is that our sample is not uniformly distributed in the disk. Some azimuth intervals have large concentrations of H II regions (e.g., 350°–20°), while others have no objects at all (see Fig. 2). We divided our H II region sample into four azimuth ranges chosen such that each contains a comparable number of nebulae: 300°–30°, 30°–90°, 90°–150°, and 150°–215° (G49.582−0.38 and G5.956−1.265 are not included in this analysis).

Most of the intervals are relatively well populated between $R_{\rm Gal} = 2$ and 10 kpc. Because of this, we fit the T_e^* gradient over a shorter $R_{\rm Gal}$ interval, roughly from 3 to 9 kpc. Properties of the gradient fits are given in Table 4 for each azimuth interval. (Table 4 gives the same fit information as Table 3.) There is a variation in the T_e^* gradient derived for the different azimuth ranges. It is impossible, however, for us to draw any significant astrophysical inferences from this result because the azimuth ranges do span different angular zones, cover different $R_{\rm Gal}$ ranges, and contain different numbers of nebulae.

In summary, we find no definitive evidence for clumpiness or azimuthal variations in the distribution of nebular electron temperatures. A much larger H II region sample that is more uniformly distributed in the Milky Way disk is needed.

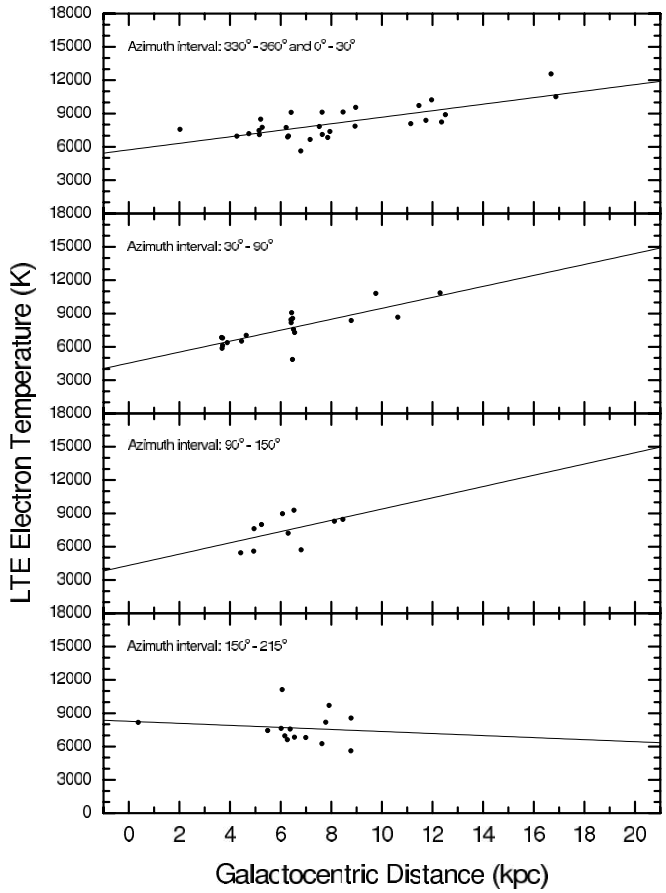

FIG. 7.—Nebular electron temperature plotted as a function of Galactocentric radius for four distinct ranges of Galactocentric azimuth. The analysis is compromised because our H II region sample is not uniformly distributed in the Milky Way's disk (see Fig. 2).

5.4. *Comparison with Other Milky Way Electron Gradient Studies*

We searched the literature for previous determinations of the electron temperature gradient in the Galactic disk. Table 5 summarizes the results of these efforts. Besides the reference for and gradient found by each study, Table 5 lists the Galactocentric distance interval together with the assumed radius of the solar orbit, $\Delta R_{\rm Gal}(R_0)$, the number, N, of objects, as well as the type of observation and analysis method used to derive the gradient. Most studies of gradients in electron temperature in the Milky Way are based on observations of RRLs. These RRL gradients vary from 250 to 440 K kpc^{-1}. WWB83 suggested a gradient of 270 K kpc^{-1} based on observations of the 76α line for 84 H II regions.

SMNDP83 derived electron temperature and abundance gradients that have often been used as the basis of many models for the chemical evolution of our Galaxy (e.g., Tosi 1988; Giovagnoli & Tosi 1995; Thon & Meusinger 1998). Because their gradient, 433 ± 40 K kpc^{-1}, is one of the steepest values ever determined, here we try to understand why this is so.

Different adopted distances are one possible source of disagreement. The SMNDP83 distances were derived from the measured radial velocities using the Schmidt (1965) rotation curve with $R_0 = 10$ kpc. According to the authors, their $R_{\rm Gal}$ distances should be accurate to within 1–2 kpc in most cases. There are a few objects in common with our sample that have $R_{\rm Gal}$ differences much larger than that expected from the change in Galactic rotation parameters and rotation curves. For example, G1.13−0.1

TABLE 4

T_e^* Gradient Fits: $T_e^* = a_1 + a_2 R_{\rm Gal}$ for Different Azimuth Intervals

Azimuth Range (deg)	a_1 (K)	a_2 (K kpc^{-1})	r	χ^2	N	$\Delta R_{\rm Gal}$ (kpc)
330–30	5730 ± 480	294 ± 53	0.73	997	29	2.0–16.9
	6070 ± 1070	233 ± 157	0.33	970	20	3.0–9.0
30–90	4540 ± 650	493 ± 95	0.79	1010	18	3.7–12.3
	4830 ± 950	432 ± 168	0.58	990	15	3.7–9.0
90–150	4320 ± 2050	507 ± 324	0.48	1320	10	4.4–8.5
	4320 ± 2050	507 ± 324	0.48	1320	10	4.4–8.5
150–215	8270 ± 1360	−92 ± 200	−0.13	1481	14	0.4–8.8
	8500 ± 2910	−120 ± 410	−0.09	1546	13	3.0–8.8

Note.—QF = *A*, *B*, and *C*, without the outliers G49.582−0.38 and G5.956−1.265.

is placed at $R_{\rm Gal} \approx 6.0$ kpc in SMNDP83, whereas we derive a distance of $R_{\rm Gal} \approx 0.1$ kpc. Rudolph et al. (1997) gave $R_{\rm Gal} \approx 0.91$ kpc for this H II region (Lis 1991; Simpson & Rubin 1990). Distances for G0.6−0.6 are also quite different. One way to compare our results to SMNDP83's is to consider only the group of 22 H II regions in common. If we adopt their distances for these 22 sources, our electron temperature gradient steepens from 258 ± 50 to 363 ± 37 K kpc^{-1}, which is still far short of the 433 ± 40 K kpc^{-1} SMNDP83 result.

The SMNDP83 source sample consists of 67 distinct Galactic H II regions located in the range $R_{\rm Gal} = 3.5$–13.7 kpc. The RRL data for 44 H II regions were their own 5 GHz (H109α) observations. This was supplemented by 14.7 GHz (H76α) observations of 23 southern H II regions by McGee & Newton (1981). All these observations were made with the Parkes 64 m radio telescope.

We compare our T_e^* results with those of SMNDP83 in Figure 8, where temperatures derived from the H76α and H109α lines are plotted with different symbols (*triangles and circles*, respectively). To avoid the distance issue, we used their measured velocities to derive new kinematic values for $R_{\rm Gal}$ in exactly the same way that we derived our own distances. We show only those points for which we could recompute the SMNDP83 $R_{\rm Gal}$. Our new distances (as well as most of the original SMNDP83 distances) were calculated using Galactic rotation curves derived from northern hemisphere data. North-south symmetries in Galactic rotation have long been known (e.g., Burton 1988), so it might not be appropriate to use our adopted rotation curve for distances to fourth-quadrant H II regions. Fourth-quadrant sources make up most of the SMNDP83 sample for $R_{\rm Gal} > 6$ kpc.

Figure 8 shows that the electron temperatures obtained using the H76α data are completely consistent with our results. The discordance between our work and that of SMNDP83 arises mostly from the low-temperature points calculated with the H109α lines located between $R_{\rm Gal} = 4$ and 6 kpc. Deharveng et al. (2000) also noted that the SMNDP83 electron temperatures in the $R_{\rm Gal} =$ 3–7 kpc zone are generally lower than those derived by other RRL studies (Mezger et al. 1979; WWB83; Caswell & Haynes 1987).

There are at least three factors that could steepen the SMNDP83 gradient: a systematic difference between the T_e derived from the H76α and H109α lines, a change in distance scales at roughly $R_{\rm Gal} > 6$ kpc, or a different abundance gradient for fourth-quadrant H II regions.[9]

We also compare our results with those by Afflerbach et al. (1996), who measured electron temperatures in ultracompact H II

[9] We find an indication of just this for our fourth-quadrant nebular sample shown in Fig. 7.

TABLE 5

Comparison of Electron Temperature Gradient Determinations

Reference	$\Delta R_{\rm Gal}$ (R_0)	$dT_e/dR_{\rm Gal}$	N	Observation	Method
PTR78	8.4–13.9 (10.0)	1100	5	Optical	[O III] $\lambda\lambda$4363, 5007
LRC79	5.0–13.0 (10.0)	390 ± 70	20	RRL	T_L(H86α)/T_C
LRC79	5.0–13.0 (10.0)	250 ± 150	20	RRL	T_L(H108β)/T_C
WBW79	5.0–12.5 (10.0)	400 ± 100	18	RRL	T_L(H65α)/T_C
DWBW80	4.0–9.0 (10.0)	340 ± 90	115[a]	RRL	T_L(H110α)/T_C
MN81	5.0–11.0 (10.0)	420	23	RRL	T_L(H76α)/T_C
GR83	3.6–12.6 (10.0)	440 ± 50	23	RRL	T_L(H125α)/T_C
SMNDP83	3.5–13.7 (10.0)	433 ± 40	67	RRL	T_L(H109α, H76α)/T_C
WWB83	4.0–17.0 (10.0)	270	84	RRL	T_L(H76α)/T_C
ACC85	4.0–12.0 (10.0)	310	27	RRL	T_L(H166α)/T_C
ACA96	4.0–11.0 (8.5)	320 ± 64	17	UC RRL	T_L(H66α, H76α, H93α)/T_C
DPCC00	6.6–14.8 (8.5)	372 ± 38	6[b]	Optical, RRL	[O III] $\lambda\lambda$4363, 5007, T_L/T_C
This work	0.0–17.0 (8.5)	287 ± 46	76	RRL	T_L(H91α)/T_C
This work (− GC)	2.0–17.0 (8.5)	340 ± 45	73	RRL	T_L(H91α)/T_C

[a] Objects averaged in six groups, corresponding to increments of 1 kpc in Galactocentric radius.

[b] T_e([O III]) in six H II regions plus mean temperatures obtained, in 1 kpc bins, from the following RRL studies: Mezger et al. (1979), SMNDP83, WWB83, and Caswell & Haynes (1987).

References.—ACA96: Afflerbach et al. 1996; ACC85: Azcárate et al. 1985; DPCC00: Deharveng et al. 2000; DWBW80: Downes et al. 1980; GR83: Garay & Rodríguez 1983; LRC79: Lichten et al. 1979; MN81: McGee & Newton 1981; PTR78: Peimbert et al. 1978; SMNDP83: Shaver et al. 1983; WBW79: Wilson et al. 1979; WWB83: Wink et al. 1983.

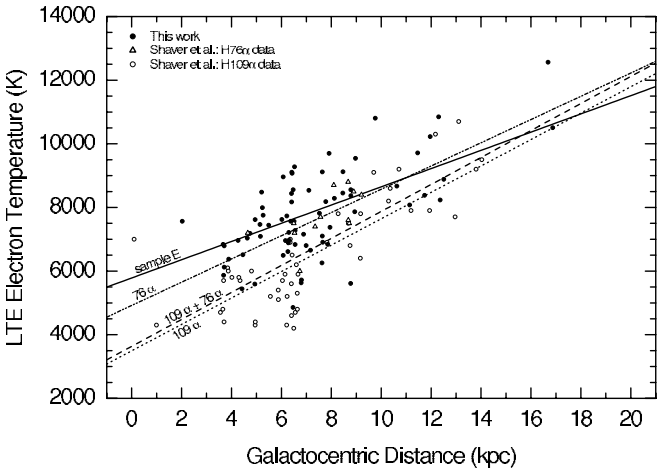

FIG. 8.—Comparison of our H II region electron temperatures with those from SMNDP83. The SMNDP83 nebulae were observed with the H76α (*triangles*) and H109α (*circles*) recombination lines. Their sample has a large number of objects in the interval $R_{\rm Gal} = 2$–6 kpc. Their H109α T_e^* values in this zone are systematically lower than ours, which may contribute to the very steep electron temperature gradient they derived.

regions using the H42α, H66α, H76α, and H93α RRLs. They found a Galactocentric gradient $T_e = (320 \pm 64)R_{\rm Gal} + (5537 \pm 387)$ K, which is in good agreement with our value despite the fact that ultracompact H II regions are much denser nebulae than our sources.

Optical studies of Galactic-scale H II region electron temperature gradients are difficult because dust in the Galactic plane causes high extinction in the visible. Optical observations by Peimbert et al. (1978) gave a large gradient of $\sim$1100 K kpc^{-1}. Their result was probably influenced by the short $R_{\rm Gal}$ interval spanned by their sample. A more recent optical estimate by Deharveng et al. (2000) yields a gradient consistent with that obtained by RRL methods. Finally, radio continuum observations at low radio frequency by Omar et al. (2002) are also consistent with the gradient estimated by Deharveng et al. (2000) for the $R_{\rm Gal}$ interval spanning 10–18 kpc (albeit for a much smaller sample).

Maciel & Faúndez-Abans (1985) investigated the radial electron temperature gradient for a large sample of Peimbert (1978) type II planetary nebulae (PNe) using electron temperatures derived from forbidden lines of [O III]. Because type II PNe have approximately circular orbits and thus do not appreciably change their Galactocentric distances during their lifetimes, they are well suited to abundance-gradient studies. The observed scatter in T_e is larger than that for H II regions, probably due to the large range of effective temperatures of the central stars, winds, optical depth effects, etc. Nonetheless, Maciel & Faúndez-Abans (1985) found a correlation between the electron temperature and Galactocentric distance for type II PNe with a gradient of order 600 K kpc^{-1} and an uncertainty of about 20%.

Compared to these much older PNe, H II regions are of zero age and thus sample the physical state of the current interstellar medium. Thus, the flattening of the T_e versus $R_{\rm Gal}$ gradient seen when one compares the PNe and H II regions may be caused by Galactic-scale temporal chemical evolution. This time flattening of the electron temperature gradient should be accompanied by a corresponding time flattening of the abundance gradient. In fact, such a flattening based on the comparison of data from several types of objects (planetary nebulae, H II regions, open clusters, Cepheids, and young stars) has been proposed by Maciel et al. (2003, 2005, 2006). It is also predicted by some recent inside-out formation scenario chemical evolution models (Hou et al. 2000; Alibés et al. 2001).

6. DISCUSSION

6.1. *The Electron Temperature of Galactic* H II *Regions*

The electron temperature of an H II region in thermal equilibrium is set by the balance of competing heating and cooling mechanisms. It is therefore somewhat surprising that there is a Galactic T_e gradient. There are at least four physical properties that could affect T_e: (1) the effective temperature of the ionizing star, $T_{\rm eff}$, which sets the hardness of the radiation field exciting (and heating) the nebula; (2) the electron density—collisional de-excitation in the high n_e H II region will inhibit cooling and increase T_e; (3) dust grains that affect the heating and cooling in complex ways; and (4) heavy-element abundance, which increases cooling and decreases T_e (Garay & Rodríguez 1983).

Rubin (1985) explored how metallicity, gas density, and the stellar effective temperature affect the average electron temperature in model H II regions. These models predict changes in T_e of 7000 K for a factor of 10 change in metal abundance, 2900 K for a change in density from 100 to 10^5 cm^{-3}, and 1300 K for a change in $T_{\rm eff}$ from 33,000 to 45,000 K (B0 to O5 spectral type). Dust grains are known to play a significant role in the heating and cooling of H II regions (e.g., Mathis 1986; Baldwin et al. 1991; Shields & Kennicutt 1995). Photoelectric heating occurs as electrons are ejected from dust grains while the gas is cooled by the collisions of fast particles with grains. The electron temperature will decrease with distance from the star as the ionizing radiation field is attenuated by dust grains. But the electron temperature will also increase as coolants are depleted onto dust grains. Taking these competing factors into account, Oliveira & Maciel (1986) concluded that dust grains do not significantly contribute to the observed T_e gradient with a maximum variation of 500 K. Therefore, metallicity is the most sensitive factor that sets the nebular T_e value, so H II region metal abundance variations are the best interpretation for the observed T_e gradient.

The electron temperature need not be a constant, however, and the observational methods used to determine T_e are sensitive to different regions of the nebula. The two main methods used to determine electron temperatures in H II regions are (1) recombination line-to-continuum ratios, such as hydrogen RRL and continuum emission; and (2) forbidden line ratios, such as the ratio [O III]λ4363/(λ4959 + λ5007). The recombination line method is weighted toward the lower temperature regions with a weak dependence on T_e, while the forbidden line method is weighted toward the higher temperature regions with a strong dependence on T_e (e.g., Peimbert 1967). Therefore, if temperature structure exists in H II regions, these methods can produce different electron temperatures. Observations of [O III] and oxygen recombination lines in Orion show such temperature fluctuations (Esteban et al. 1998).

Comparison of hydrogen RRL and [O III] electron temperatures is more complicated, since the emission lines arise from different species. The intensities of the RRLs of H relative to the underlying continuum, for example, should give an estimate of the electron temperature in the whole ionized H region (H^+ zone), while observations of the [O III] optical emission should give an estimate of the electron temperature in the O^{++} zone. Photoionization models indicate that the electron temperature should be higher in the outer regions, since the ionizing radiation becomes harder with distance from the exciting star and the very efficient coolants such as O^{++} are located close to the exciting star

(Stasińska 1980; Garnett 1992). This suggests that $T_e(O^{++}) \leq T_e(H^+) \leq T_e(O^+)$ (Stasińska 1990; Stasińska & Shaerer 1997; Deharveng et al. 2000). The temperature measured via the RRL, however, is not strictly $T_e(H^+)$, and that measured with the optical [O III] forbidden lines is not strictly $T_e(O^{++})$. Because the recombination lines are emitted preferentially in low-temperature regions, $T_e(\text{radio}) \leq T_e(H^+)$, and because the optical forbidden lines are enhanced in high-temperature regions, $T_e([O\ III]) \geq T_e(O^{++})$. Despite this complexity, the electron temperatures determined by these two methods toward the same H II region produce values of T_e that are similar to within the uncertainties (Deharveng et al. 2000).

WWB83 found no correlation between T_e and either the Lyman continuum flux, N_L, used to probe different stellar effective temperatures, or the electron density, n_e. Theoretically, higher values of N_L and n_e should increase T_e (Rubin 1985). But there are H II regions with high N_L and low n_e (e.g., the Rosette Nebula) that will increase the scatter in any such analysis. SMNDP83 found a correlation with T_e by dividing the H II regions into two groups of either high or low values of *both* N_L and n_e. But the correlation seems weak, since many of the points at smaller R_{Gal}, where the correlation is best, are nebulae that appear to have systematically lower electron temperatures (i.e., the H109α survey sources). The ultracompact H II region survey of Afflerbach et al. (1996) probes nebulae of much higher electron density than other surveys. Because these observations were made with an interferometer, any diffuse gas within their primary beam will be spatially filtered. Their derived electron temperatures are higher by $\sim$1000 K compared with other surveys of classical H II regions.

We explored the effects of N_L and n_e on electron temperature in our sample and find no correlation. We used an approach similar to SMNDP83; sources were selected either below or above a threshold value of the excitation and electron density [$\log(N_L) = 49.5\ s^{-1}$ and $n_e = 150\ cm^{-3}$]. RRL and continuum surveys of classical H II regions with single-dish telescopes probe H II region complexes that typically contain more than one ionizing star with different spectral types. Such regions consist of both low- and high-density gas (e.g., Balser et al. 1999). But does this account for the observed dispersion of the T_e gradient as has been suggested (e.g., SMNDP83)?

Another possibility is that the dispersion is caused by variations in metallicity. After all, stellar abundances at a given R_{Gal} show a dispersion in abundance. Interpretation of the stellar abundances is complicated because samples typically contain stars of varying age that may well have been formed at a different R_{Gal} than their current location (Edvardsson et al. 1993). Correcting for birth location and age, Edvardsson et al. (1993) found a scatter of 0.5 dex in the solar neighborhood. Friel et al. (2002) found a scatter of about half that in disk star cluster abundances. A scatter of 0.3 dex in heavy-element abundance produces a scatter of 2000 K in T_e, entirely consistent with our observed scatter.

For H II regions, Mehringer et al. (1993) suggested differences in metallicity as the best candidate for the $\sim$2000 K change in T_e between components 1 and 2 in the Sgr B complex. Since our survey spans a large region of the Galaxy, both radially and azimuthally, we were able to explore such effects by comparing T_e at a given R_{Gal} over a large range of azimuth. The results were inconclusive. Sensitive RRL observations in critical areas of the Galaxy could reveal such variations and place important constraints on Galactic chemical evolution models.

6.2. *The Galactic Center*

Our nebular sample F fit to the electron temperature gradient excludes the Galactic center (GC) sources Sgr B2 and G1.13−0.1 and includes the outer Galaxy nebulae S209 and S209 N. This sample produces the steepest T_e^* gradient, thus providing an extreme constraint on Galactic chemical evolution models.

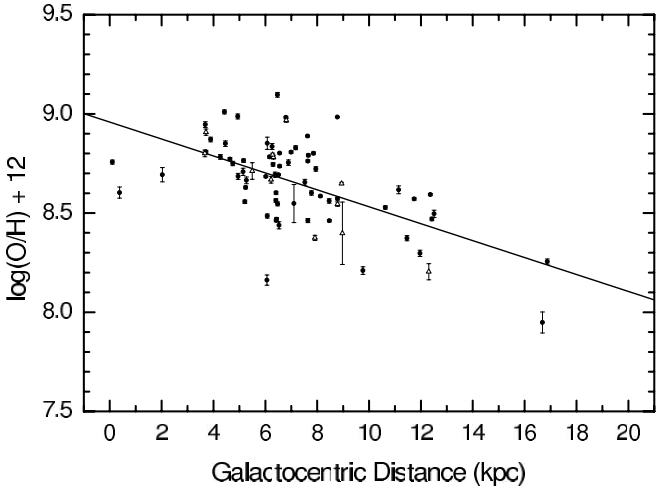

FIG. 9.—Galactic O/H abundance gradient derived from our nebular electron temperatures, using the relation between O/H and T_e of SMNDP83. Symbols have the same meaning as in Fig. 3. The solid line is the eq. (6) least-squares fit.

Early RRL observations of H II regions in the GC produced electron temperatures that were higher than those expected from an extrapolation of the electron temperature gradient in the Galactic disk (Mezger et al. 1979; Downes et al. 1980; WWB83). Since the chemical evolution of the GC may be different than the disk, it is not surprising that electron temperatures in the GC do not follow the gradient in the disk. Higher spatial resolution observations reveal a wide range of electron temperatures ($\sim$4000–10,000 K) in GC H II regions (Roelfsema et al. 1987; Gaume & Claussen 1990; Mehringer et al. 1992, 1993; De Pree et al. 1995, 1996; Lang et al. 1997, 2001). The large range of electron temperatures may be due to the complexity of the GC. Real variations in metallicity, electron density, and excitation will affect T_e. Some of the higher electron temperatures are overestimated when the radio continuum is contaminated with nonthermal emission. Nevertheless, in some objects, very high electron temperatures ($T_e \sim 20{,}000$ K) appear to be real where the gas may not be in equilibrium (Mehringer et al. 1995). Since the zero level for our radio continuum temperature was determined away from the thermal object but not far from the Galactic disk, any smooth nonthermal emission should have been removed.

6.3. *The Galactic* O/H *Abundance Gradient*

The electron temperature may be converted to oxygen abundance using a correlation between metal abundance and temperature. Because of the broad interest in abundance gradients, we provide here one such conversion of our T_e^* gradient to an O/H gradient, deferring a more extended discussion to a future paper. Using the relation between O/H and T_e of SMNDP83 yields the result shown in Figure 9. The O/H gradient is about -0.04 dex kpc^{-1}, in agreement with results from Afflerbach et al. (1996), Deharveng et al. (2000), Pilyugin (2003), and Esteban et al. (2005). The exact fit to the 76 sample E nebulae in Figure 9 is

$$\log(O/H) + 12 = (8.958 \pm 0.052) + (-0.043 \pm 0.007) R_{Gal}\ \text{kpc}, \quad (6)$$

with a correlation coefficient of $r = -0.59$. If our observed T_e^* dispersion of $\sim$1100 K is caused by real abundance fluctuations,

then this would correspond to an [O/H] abundance dispersion of $\sim$0.16 dex.

7. SUMMARY

We used extremely sensitive RRL observations of a large sample of Galactic H II regions to study the nebular electron temperature gradient in the Milky Way disk. LTE electron temperatures were derived from the observed H91α RRL-to-continuum intensity ratios. Departures from LTE were found to be small, given the properties of our H II regions and the fact that at 8.6 GHz the effect of pressure broadening is not large. Our 109 source sample consists mostly of classical H II regions of low density and with angular sizes larger than the 3.′20 telescope beam.

Our temperature gradient analysis has the following virtues:

1. We analyze a large sample of H II regions spanning the entire Galactic disk from $R_{\rm Gal} = 0$ to 17 kpc.
2. We use high-sensitivity RRL measurements obtained with very long integration times for our derivation of the electron temperature.
3. All nebular Galactocentric distances are calculated kinematically in a self-consistent way.
4. All of the data were observed with the same telescope (the NRAO 140 ft), identically calibrated, and analyzed in a uniform, self-consistent way.

Our best estimate of the electron temperature gradient is derived from a sample of 76 sources for which we have the highest quality data (sample E in Table 3). We conclude that the present gradient in electron temperature in the Galactic disk has a minimum at the Galactic center and rises at a rate of 287 ± 46 K kpc^{-1}. This value is consistent with determinations in the optical by Deharveng et al. (2000) and in the radio by WWB83, Afflerbach et al. (1996), and Azcárate et al. (1985). Our gradient is about a factor of 2 less steep than the gradient proposed by SMNDP83.

We find little if any variation of the electron temperature gradient with Galactocentric distance. There is some variation of the temperature gradient calculated for different regions of Galactocentric azimuth. Unfortunately, our nebular sample is not homogeneously distributed in the Galactic plane, which complicates this analysis; thus, no firm conclusions can be drawn.

The scatter we find in the H II region electron temperatures at a given Galactocentric radius is not due to observational error, but rather to intrinsic fluctuations in these temperatures that are almost certainly due to fluctuations in the nebular heavy-element abundances. A comparison of the H II region gradient with a much steeper gradient found for planetary nebulae suggests that the electron temperature gradient evolves with time, becoming flatter as a consequence of the chemical evolution of the Milky Way's disk.

We thank the staff of NRAO, Green Bank, for their help, support, and friendship. The ^{3}He research has been supported, in part, by the National Science Foundation. The most recent grants were AST 00-98047 to T. M. B. and AST 00-98449 to R. T. R. We thank Butler Burton and Eileen Friel for discussions that have improved this effort. The perceptive comments made by our anonymous referee helped us to improve this paper. C. Q. is grateful to the department of astronomy at the University of Virginia for its hospitality. Her work was partially supported by the Levinson Fund of the Peninsula Community Foundation, Fundação de Amparo à Pesquisa do Estado de São Paulo (FAPESP), and Conselho Nacional de Desenvolvimento Científico e Tecnológico (CNPq/MCT).

REFERENCES

Afflerbach, A., Churchwell, E., Acord, J. M., Hofner, P., Kurtz, S., & De Pree, C. G. 1996, ApJS, 106, 423 (ACA96)
Alibés, A., Labay, J., & Canal, R. 2001, A&A, 370, 1103
Altenhoff, W. J., Downes, D., Pauls, T., & Schraml, J. 1979, A&AS, 35, 23
Azcárate, I. N., Cersosimo, J. C., & Colomb, F. R. 1985, Rev. Mex. AA, 10, 179 (ACC85)
Baldwin, J. A., Ferland, G. J., Martin, P. G., Corbin, M. R., Cota, S. A., Peterson, B. M., & Slettebak, A. 1991, ApJ, 374, 580
Balser, D. S. 1995, Ph.D. thesis, Boston Univ.
Balser, D. S., Bania, T. M., Brockway, C. J., Rood, R. T., & Wilson, T. L. 1994, ApJ, 430, 667
Balser, D. S., Bania, T. M., Rood, R. T., & Wilson, T. L. 1999, ApJ, 510, 759 (BBRW99)
Bania, T. M., Balser, D. S., Rood, R. T., Wilson, T. L., & Wilson, T. J. 1997, ApJS, 113, 353
Bania, T. M., Rood, R. T., & Wilson, T. L. 1987, ApJ, 323, 30
Brand, J., & Blitz, L. 1993, A&A, 275, 67
Burton, W. B. 1988, Galactic and Extragalactic Radio Astronomy (Berlin: Springer), 295
Caswell, J. L., & Haynes, R. F. 1987, A&A, 171, 261
Churchwell, E., Mezger, P. G., & Huchtmeier, W. 1974, A&A, 32, 283
Churchwell, E., Smith, L. F., Mathis, J., Mezger, P. G., & Huchtmeier, W. 1978, A&A, 70, 719
Churchwell, E., & Walmsley, C. M. 1975, A&A, 38, 451
Clemens, D. P. 1985, ApJ, 295, 422
Deharveng, L., Peña, M., Caplan, J., & Costero, R. 2000, MNRAS, 311, 329 (DPCC00)
De Pree, C. G., Gaume, R. A., Goss, W. M., & Claussen, M. J. 1995, ApJ, 451, 284
———. 1996, ApJ, 464, 788
Downes, D., Wilson, T. L., Bieging, J., & Wink, J. 1980, A&AS, 40, 379 (DWBW80)
Edvardsson, B., Andersen, J., Gustafsson, B., Lambert, D. L., Nissen, P. E., & Tomkin, J. 1993, A&A, 275, 101
Esteban, C., García-Rojas, J., Peimbert, M., Peimbert, A., Ruiz, M. T., Rodríguez, M., & Carigi, L. 2005, ApJ, 618, L95 (EGPPRR05)
Esteban, C., Peimbert, M., Torres-Peimbert, S., & Escalante, V. 1998, MNRAS, 295, 401
Fich, M., & Silkey, M. 1991, ApJ, 366, 107
Friel, E. D., Janes, K. A., Tavarez, M., Scott, J., Katsanis, R., Lotz, J., Hong, L., & Miller, N. 2002, AJ, 124, 2693
Fürst, E., Reich, P., & Reif, K. 1990, A&AS, 85, 691
Garay, G., & Rodríguez, L. F. 1983, ApJ, 266, 263 (GR83)
Garnett, D. R. 1992, AJ, 103, 1330
Gaume, R. A., & Claussen, M. J. 1990, ApJ, 351, 538
Giovagnoli, A., & Tosi, M. 1995, MNRAS, 273, 499
Goldberg, L. 1968, in Interstellar Ionized Hydrogen, ed. Y. Terzian (New York: Benjamin), 373
Hachisuka, K., et al. 2006, ApJ, 645, 337
Haynes, R. F., Caswell, J. L., & Simons, W. J. 1978, Australian J. Phys. Astrophys. Suppl., 45, 1
Hou, J. L., Prantzos, N., & Boissier, S. 2000, A&A, 362, 921
Kuchar, T. A., & Bania, T. M. 1990, ApJ, 352, 192
Lang, C. C., Goss, W. M., & Morris, M. 2001, AJ, 121, 2681
Lang, C. C., Goss, W. M., & Wood, D. O. S. 1997, ApJ, 474, 275
Lichten, S. M., Rodríguez, L. F., & Chaisson, E. J. 1979, ApJ, 229, 524 (LRC79)
Lis, D. C. 1991, ApJ, 379, L53
Maciel, W. J., Costa, R. D. D., & Uchida, M. M. M. 2003, A&A, 397, 667
Maciel, W. J., & Faúndez-Abans, M. 1985, A&A, 149, 365
Maciel, W. J., Lago, L. G., & Costa, R. D. D. 2005, A&A, 433, 127
———. 2006, A&A, 453, 587
Mathis, J. S. 1986, PASP, 98, 995
McGee, R. X., & Newton, L. M. 1981, MNRAS, 196, 889 (MN81)
Mehringer, D. M., De Pree, C. G., Gaume, R. A., Goss, W. M., & Claussen, M. J. 1995, ApJ, 442, L29
Mehringer, D. M., Palmer, P., Goss, W. M., & Yusef-Zadeh, F. 1993, ApJ, 412, 684
Mehringer, D. M., Yusef-Zadeh, F., Palmer, P., & Goss, W. M. 1992, ApJ, 401, 168
Mezger, P. G., & Henderson, A. P. 1967, ApJ, 147, 471
Mezger, P. G., Pankonin, V., Schmid-Burgk, J., Thum, C., & Wink, J. 1979, A&A, 80, L3

Oliveira, S., & Maciel, W. J. 1986, Ap&SS, 128, 421
Omar, A., Chengalur, J. N., & Anish Roshi, D. 2002, A&A, 395, 227 (OCAR02)
Osterbrock, D. E., & Flather, E. 1959, ApJ, 129, 26
Panagia, N., & Walmsley, C. M. 1978, A&A, 70, 411
Peimbert, M. 1967, ApJ, 150, 825
———. 1978, IAU Symp. 76, Planetary Nebulae, ed. Y. Terzian (Dordrecht: Reidel), 215
Peimbert, M., Rayo, J. F., & Torres-Peimbert, S. 1978, ApJ, 220, 516 (PTR78)
Peimbert, M., Rodríguez, L. F., Bania, T. M., Rood, R. T., & Wilson, T. L. 1992, ApJ, 395, 484
Pilyugin, L. S. 2003, A&A, 399, 1003
Quireza, C., Rood, R. T., Balser, D. S., & Bania, T. M. 2006, ApJS, 165, 338
Reich, W., Fürst, E., Reich, P., & Reich, K. 1990, A&AS, 85, 633
Roelfsema, P. R., Goss, W. M., Whiteoak, J. B., Gardner, F. F., & Pankonin, V. 1987, A&A, 175, 219
Rohlfs, K., & Wilson, T. L. 2000, Tools of Radio Astronomy (New York: Springer)
Rood, R. T., Bania, T. M., & Wilson, T. L. 1984, ApJ, 280, 629
Rubin, R. H. 1985, ApJS, 57, 349
Rubin, V. C., Kumar, C. K., & Ford, W. K., Jr. 1972, ApJ, 177, 31
Rudolph, A. L., Simpson, J. P., Haas, M. R., Erickson, E. F., & Fich, M. 1997, ApJ, 489, 94
Schmidt, M. 1965, in Galactic Structure, ed. A. Blaauw & M. Schmidt (Chicago: Univ. Chicago Press), 513
Searle, L. 1971, ApJ, 168, 327
Shaver, P. A. 1980, A&A, 91, 279
Shaver, P. A., McGee, R. X., Newton, L. M., Danks, A. C., & Pottasch, S. R. 1983, MNRAS, 204, 53 (SMNDP83)
Shaver, P. A., & Wilson, T. L. 1979, A&A, 79, 312
Shields, J. C., & Kennicutt, R. C., Jr. 1995, ApJ, 454, 807
Simpson, J. P., & Rubin, R. H. 1990, ApJ, 354, 165
Smith, H. E. 1975, ApJ, 199, 591
Stasińska, G. 1980, A&A, 85, 359
———. 1990, A&AS, 83, 501
Stasińska, G., & Schaerer, D. 1997, A&A, 322, 615
Thon, R., & Meusinger, H. 1998, A&A, 338, 413
Thum, C., Mezger, P. G., & Pankonin, V. 1980, A&A, 87, 269 (TMP80)
Tosi, M. 1988, A&A, 197, 47
Wilson, T. L., Bieging, J., & Wilson, W. E. 1979, A&A, 71, 205 (WBW79)
Wink, J. E., Wilson, T. L., & Bieging, J. H. 1983, A&A, 127, 211 (WWB83)
Xu, Y., Reid, M. J., Zheng, X. W., & Menten, K. M. 2006, Science, 311, 54